Thermal navigation in larval zebrafish

Thermal navigation in larval zebrafish

A dissertation presented

by

Drew Norman Robson

to

The Department of Molecular and Cellular Biology

In partial fulfillment of the requirements
for the degree of
Doctor of Philosophy
in the subject of

Biology

Harvard University
Cambridge, Massachusetts

January 2013

Professors Alexander F. Schier and Florian Engert

Drew Norman Robson

Thermal navigation in larval zebrafish

Abstract

Navigation in complex environments requires selection of appropriate actions as a function of local cues. To gain a quantitative and mechanistic understanding of zebrafish thermal navigation, we have developed a novel assay that requires animals to rely exclusively on thermosensory information in the absence of other cues such as vision or mechanosensation. We show that zebrafish use both absolute and relative temperature information to restrict their locomotor trajectories to a preferred temperature range. We identify components of movement that are modulated solely by absolute temperature, as well as components that are modulated by both absolute and relative temperature. Specifically, we find that dwell time between movements and displacement per movement depend solely on absolute temperature, whereas turn magnitude and turn direction bias are modulated by absolute and relative temperature. To evaluate whether these sensorimotor relationships could explain thermal restriction in our navigation assay, we performed Monte Carlo simulations of locomotor trajectories based on all or subsets of these relationships. We find that thermosensory modulation of turn magnitude and turn direction bias constitute the core navigation strategy in larval zebrafish, while modulation of dwell time accelerates the execution of this strategy at noxious temperatures. Modulation of turn direction bias represents a novel strategy not found in invertebrate models, whereby animals correct unfavorable headings by preferentially turning in a preferred turn direction until they obtain a favorable heading. Modulating turn direction bias in response to recent sensory experience is an effective strategy for selecting favorable headings in organisms that do not have a dedicated sampling phase before each reorientation event.

Table of Contents

List of Figures

Acknowledgements

I am extremely grateful to Alex for his openness in allowing me to explore a new direction, and for being incredibly patient while the project took shape. Alex's lab is a microcosm of innovation and collaboration, and he has a unique talent for providing structure and flexibility in a lab that is widely diverse and yet feels tightly integrated. I could not have asked for a better environment in which to grow and mature as a scientist.

Florian's passion for physics and his valiant attempts to preach its virtues to the lab has influenced how I think about my projects. I have also benefited greatly from a culture of invention that started with Adam Kampff and continues to run deep in the Engert lab.

I would like to thank all members of my committee for invaluable feedback. Former committee members include Markus Meister, Venki Murthy, and Sharad Ramanathan, and my final committee members are Josh Sanes, Aravi Samuel, and Bence Olveczky. All have contributed in some way. I am grateful to Sharad for prompting me to think harder about the issue of convection in my chamber designs. I am indebted to Aravi for his pioneering work in the thermotaxis field. His model of Drosophila thermotaxis is undoubtedly an inspiration for my current project. Above all, I am grateful to Josh for being a constant voice of reason these last five years. Josh really helped redefine the direction of the project when it needed it the most. He's a tough guy to please, and I wouldn't have it any other way.

I'd like to thank all the members of the Schier and Engert labs for providing inspiration, feedback and support. I honestly could not have done it without them.

Finally, I would like to thank Jennifer Li. She has contributed equally to all aspects of this project. Where there was one pair of footprints in the sand, they were surely Jen's.

1. Introduction

1 ABSTRACT

Given the profound effects that temperature can have on chemical reactions and physical processes, it is perhaps not surprising that biological systems have evolved compensatory mechanisms to mitigate the effects of temperature. These adaptations span every conceivable level, from highly conserved molecular pathways to a wide range of behavioral strategies. The behavioral approach is particularly important for ectotherms such as unicellular organisms, invertebrates, and fish, since they lack internal homeostatic mechanisms for thermoregulation. These animals spend essentially their entire lives in thermal equilibrium with their environment, and so they must rely upon locomotion to seek out favorable temperatures. Studies of model invertebrate systems have yielded quantitative behavioral models of the strategies used by these animals for thermal navigation. Establishing precise models for the sensorimotor transformations and decision making processes during navigation has allowed the field to delve deeper into questions about implementation. In this chapter, we will review the navigation strategies employed by *E. coli*, *C. elegans*, and *Drosophila*. We will also review how genetic mutants, optical lesions, functional imaging, and optogenetics have helped to reveal how these navigation strategies are implemented in a variety of model nervous systems.

2 CHEMOTAXIS AND THERMOTAXIS IN *E. COLI*

Experiments have shown[1-2] that the unicellular bacteria *E. coli* can follow thermal gradients using essentially the same strategy and molecular machinery that underlies chemotaxis[3], which is one of the most well studied signal transduction cascades in biology[4-5]. In his pioneering study, Howard Berg showed that the *E. coli* could navigate up a concentration gradient of a chemoattractant by suppressing the rate of reorientation when solute concentration was increasing[3]. Berg recorded the locomotion of

individual cells in three dimensions and measured the spontaneous rates at which *E. coli* performed swims, in which cell move forward in a straight line, and tumbles, in which cells disperse their flagella to introduce a random reorientation to their three-dimensional heading. Importantly, Berg showed that when *E. coli* swim down the gradient of a chemoattractant the rate of tumbling is indistinguishable from the spontaneous reorientation rate in isotropic solutions. Instead, *E. coli* bias their navigation by specifically suppressing this spontaneous rate of tumbling when the chemoattractant concentration is increasing. This has the effect of prolonging runs heading up the gradient and shortening runs heading down the gradient. This process of stochastically enriching for favorable headings is called a biased random walk.

Mechanistically, the biased random walk strategy is implemented using sophisticated molecular machinery. Under isotropic conditions, the spontaneous rate of tumbling is set by an intracellular phosphorylation cascade. Briefly, the chemoreceptor-associated kinase CheA autophosphorylates itself at some basal rate and then transfers its phosphate group to the response regulator CheY. CheY-P then diffuses to the flagellar motor complex, reversing the rotation of the flagella and causing the cell to tumble. Extracellular ligand can then affect rate of tumbling by modulating the rate of CheY autophosphorylation. This modulation is mediated by integration of activity from five chemoreceptors, including Tar and Tsr, which change conformation in the ligand-bound state to reduce the rate of CheY autophosphorylation and ultimately suppress tumbling rate.

In order to maintain sensitivity to the slope of the chemical gradient over a large range of solute concentrations, *E. coli* also have an adaptation mechanism that allows them to bias their random walks over a large range of solute concentrations. This mechanism, which involves the balanced activities of the methylesterase CheB and methyltransferase CheA, allows *E. coli* to focus on relative changes in ligand concentration encountered during a run, regardless of whether the overall solute concentration is high or low. Without the adaptation mechanism, the rate of tumbling would be predominantly

controlled by absolute ligand concentration, and sensitivity to small fluctuation in gradient concentrations would be limited at high or low ligand concentrations.

Although thermotaxis in E. coli is much less studied than chemotaxis, it has been shown that E. coli can navigate thermal gradients by the same biased random walk strategy[1-2,6]. Thermosensory input is primarily transduced by the chemoreceptors Tsr and Tar. Experiments on E. coli thermotaxis in the presence of various chemoattractants indicates that the shared dependence on a common pathway causes chemotaxis and thermotaxis to interact. Ligand-induced methylation of Tsr receptors abolishes the temperature sensitivity of these receptors, while ligand-induced methylation of Tar receptors reverses the effect of temperature on the Tar receptor[1-2].

Studies of biased random walks in *E. coli* demonstrate that navigation behavior can be implemented entirely within a single cell. Unlike other implementations for thermotaxis that we will discuss later, all of which involve distributed function across a network of neurons, *E. coli* implement the entire transformation from sensory receptor to motor output using an intracellular signaling pathway.

3 THERMOSENSORY BEHAVIORS IN *C. ELEGANS*

3.1 INTRODUCTION

C. elegans currently provides the most extensively studied model of thermotaxis[7-8,9-44]. This is understandable given the many advantages of this system for combining molecular, genetic, physiological, and behavioral approaches to understanding neural networks. The entire nervous system of the adult worm comprises only 302 neurons and the complete wiring diagram has been described[45]. *C. elegans* has a short generation time, powerful genetics, and a variety of stereotyped behaviors. Despite having a relatively small nervous system, the *C. elegans* neural circuitry specifies some fairly sophisticated thermosensory behaviors. In fact, the *C. elegans* neural circuit specifies multiple modes of

thermosensory behavior, and selects between these behaviors by comparing the current temperature against an internally defined temperature called the thermotactic set-point. Briefly, the behavior of worms above the set point resembles a biased random walk, allowing animals to perform negative thermotaxis toward the set point temperature. Around the set-point temperature, worms can produce a behavior called isothermal tracking, in which they align their heading to an isotherm and actively follow it during unusually prolonged runs. Locomotion below the set-point under most conditions is atactic, resembling an unbiased random walk. The set-point itself is also complex, in that it acts as a kind of temperature memory by adapting to the recent thermal experience of the animal. In the following sections, we will review each of these behavioral features in more detail. We will then consider the insights into implementation that have been learned by a wide range of approaches, including analysis of genetic mutants, femtosecond ablation, calcium imaging in tethered and freely behaving animals, and optogenetic manipulation.

3.2 THE THERMOTAXIS SET POINT: A FORM OF LONG TERM PLASTICITY IN C. ELEGANS

C. elegans has long been known to shift its set-point for thermosensory behavior[8], but the precise relationship between the set-point, cultivation temperature, and food scarcity has only recently been clarified[26]. Although the set-point was originally described as a form of associative learning, in which animals remember the temperature at which food was last available[8], recent work has shown that the temperature set-point is constantly adapting to the temperature experienced by the animal, irrespective of food-related cues[26]. To reach these conclusions, experimenters cultivated worms overnight at 15 or 25 °C and then shifted them to the opposite temperature for varying durations of time and then finally assayed isothermal tracking to estimate the resulting set-point temperature (T_S). The experimenters found that T_S obeys first order kinetics with a time constant of approximately two hours. Importantly, they found that T_S adapts with indistinguishable kinetics whether or not food was

present at the new cultivation temperature, which shows that the mechanism of adaptation does not require association with food, as had originally been proposed. The authors also described a mutation in a diacylclycerol kinase, dgk-3, that shows superficially normal thermotaxis but has a significantly longer adaptation time in response to shifts from 15 to 25 °C. This impairment in adaptation time could be rescued by cell-specific expression of dgk-3 in the AFD neuron.

3.3 NEGATIVE THERMOTAXIS ABOVE T_C

At temperatures >2 °C above T_c, worms navigate down a thermal gradient[7-10,15,20] (**Fig. 1a**), which we refer to as negative thermotaxis. The strategy for negative thermotaxis in *C. elegans* is conceptually very similar to the biased random walk strategy first described in *E. coli*. Like *E. coli*, *C. elegans* moves continuously and its locomotion can be described as consisting of forward runs interrupted by abrupt reorientations in the form of reversal or omega turns (**Fig. 1b**). The resulting heading after an omega turn is random. When moving in a thermal gradient above the cultivation temperature, worms perform negative thermotaxis by modulating the rate of reversals and omega turns according to relative changes in temperature. Specifically, worms prolong runs heading down the gradient and interrupt runs heading up the gradient, enriching for favorable headings by a biased random walk[9,28]. Clever experiments using thermally controlled chambers or focal laser heating have shown that presenting worms with a time-varying but spatially uniform thermal waveform is sufficient to positively and negatively modulate reorientation rate[9-10,32]. These results support the simple model that worms bias their random walk based on purely temporal information. In the upcoming section on sensory imaging, we will show that a *C. elegans* thermosensory neuron effectively computes the derivative of the thermosensory input, which is the ideal signal to modulate reorientation rate in the biased random walk model.

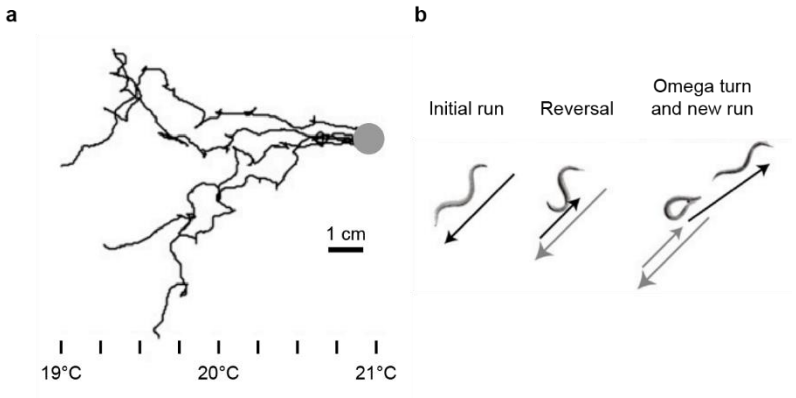

Figure 1 | *C. elegans* negative thermotaxis is a biased random walk. a, Four *C. elegans* animals performing negative thermotaxis after being placed on a thermal gradient above their cultivation temperature (15 °C). Gray circle indicates starting point. Trajectories are stochastic, but show a clear tendency to drift down the thermal gradient toward the cultivation temperature. **b,** Stereotyped motor sequence performed by *C. elegans* during negative thermotaxis. Worms move in relatively straight lines called runs, but can interrupt these runs to perform a reversal followed by an omega turn to effectively randomize the heading of the animal. Worms bias the rate of reversals based on temperature changes encountered during a run, effectively prolonging favorable runs heading down the gradient and shortening runs heading up the gradient. (Figure adapted from Garrity et al.[7])

3.4 ISOTHERMAL TRACKING NEAR T_c

Within ±2 °C of T_c, worms switch to a distinct behavioral mode called isothermal tracking in which animals run straight along isotherms while making gradual and continuous heading adjustments to follow the isotherm to within 0.1 °C[7-9,12,19-20] (**Fig. 2**). To understand isothermal tracking, we must first describe *C. elegans* in a little more detail. During forward runs, *C. elegans* actually advance by an undulating, sinusoidal motion. The head of the animal curves from side to side between successive movements. If the curves are symmetric across the left and right axis, the animal moves forward. However, in the presence of either chemical or thermal gradients, worms can bias their curving to gradually reorient toward the preferred chemical concentration or temperature. For example, to veer slightly to one side to better align with an isotherm, animals simply extend their body curvature during the phase of the undulation when they are facing toward the isotherm. The ability to continually fine-tune the heading during isothermal tracking accounts for its impressive ability to keep the animal within

0.1 °C of the isotherm. This fine tuning mechanism has been successfully modeled using a phenomenological model in which the degree of curvature is simply made directly proportional to the derivative of thermosensory input[19]. Chemotaxis appears to employ the same locomotor strategy, where it has been referred to as weathervaning[39].

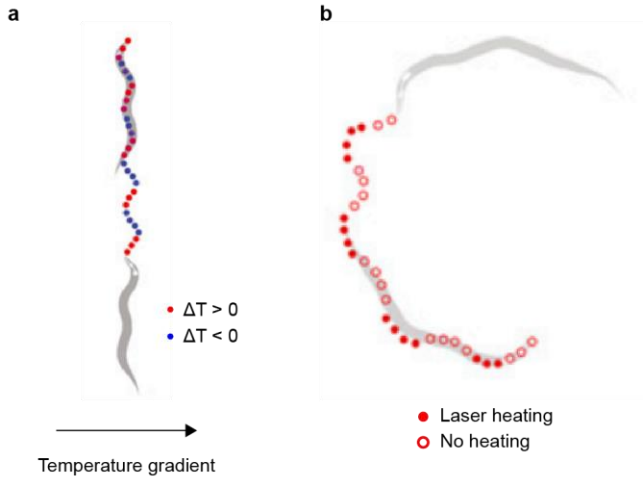

Figure 2 | During isothermal tracking, *C. elegans* actively maintains its alignment to isotherms near its T_c. a, Schematic depiction of isothermal tracking. A pair of bilateral thermosensory neurons near the nose of the animal phase-lock to the subtle temperature changes encountered during undulatory forward motion. This oscillatory signal drives directed gentle bending to maintain isothermal alignment to within 0.1 °C. **b,** Experimentally-induced steering of a freely behaving worm by applying laser-based heating to the nose of the animal during a specific phase of the undulation cycle. (Figure adapted from Garrity et al.[7])

3.5 POSITIVE THERMOTAXIS

Positive thermotaxis has been a controversial tropic in *C. elegans*. The earliest reports of thermostatic behavior in *C. elegans* suggested that *C. elegans* can navigate up or down a thermal gradient toward its preferred temperature[2,15]. More recently, however, detailed quantitative studies of thermotaxis behavior have found that positive thermotaxis is only observed within a limited range of temperatures and gradient steepness[1,4-6,11,28]. Under typical conditions in many laboratories, movement in *C. elegans* appears to be atactic[9-11], resembling an unbiased random walk.

3.6 ANALYSIS OF THERMOSENSORY BEHAVIORS BY GENETIC MUTANTS

Many of the genes shown to affect thermosensory behaviors in *C. elegans* were originally identified in screens for chemotaxis mutants[7-8,34]. These genes span a range of molecular functions, including signaling molecules and components of developmental pathways that specify the development and function of the sensory neurons and closely associated interneurons that are necessary for thermotaxis. For example, tax-2, tax-4, tax-6, and ttx-4 are genes required for intracellular signal transduction in sensory and interneurons that participate in thermotaxis. Specifically, tax-4 and tax-2 are expressed in AFD, AWC, and other sensory neurons and encode the beta and alpha subunits of a cyclic nucleotide-gated cation channel. tax-6 is expressed in AFD, AWC, and other sensory neurons, as well as interneurons and motor neurons, and encodes a subunit of Calcineurin A, an important molecule for calcium-dependent signaling. ttx-4 encodes a protein kinase C family member that expressed in sensory neurons including AFD and has a variety of roles in intracellular signal transduction within different *C. elegans* sensory neurons[46]. ttx-4 mutants are thermophilic and have severely impaired isothermal tracking. Another set of genes, such as ttx-1 and ttx-3, are required for the normal development and differentiation of cells in the thermotaxis network. ttx-1 was found to encode a member of the OTD/OTX homeodomain protein family[47]. This gene is expressed in AFD neurons and required for the normal differentiation of AFD neurons. ttx-1 mutants have strong cryophilic drive and fail to track isotherms. ttx-3 encodes a LIM homeobox gene, and ttx-3 mutants disrupt development of the AIY interneuron[48]. ttx-3 mutants are cryophilic and show severely impaired isothermal tracking.

3.7 IDENTIFYING NECESSARY CIRCUIT COMPONENTS BY FEMTOSECOND ABLATION

Although genetic analysis has strongly implicated specific neurons as having roles in the thermotaxis and isothermal tracking circuitry, such as AFD and AIY, individual mutations typically affect multiple neurons within the circuit. This lack of specificity can complicate the interpretation of the role

of individual neurons within the circuit, although cell-specific rescue certainly helps strengthen claims that a particular effect can be attributed to an individual neuron. A complementary approach to understanding the roles of individual neurons within a complex circuit is to use a femtosecond laser to ablate single neurons or defined combinations of neurons and then assay the consequences to behavior or to other parts of the circuit.

A landmark study of the roles of individual neurons in thermotaxis by femtosecond ablation revealed a number of insights into the relevant neurons for this behavior[20], although some specific results and interpretations have had to be challenged by more recent studies in light of an increasing understanding of the different modes of *C. elegans* thermosensory behavior[27]. Ablating both of the bilateral AFD neurons weakens thermotaxis and abolishes isothermal tracking, establishing its role as a major thermosensory neuron in the *C. elegans* circuit. Animals in which only one AFD neuron was ablated were still capable of performing isothermal tracking, arguing that the mechanism of isothermal tracking does not depend upon spatial comparison of the two AFD signals.

Ablation of two interneurons downstream of AFD, AIY and AIZ, established their involvement in thermosensory behaviors, although the precise phenotypes and interpretations need to be reevaluated in light of considerable progress in the field. In the original study, paired ablation of AIY gave a cryophilic phenotype, while paired ablation of AIZ gave a thermophilic phenotype. These results were interpreted as evidence that interneurons downstream of AFD, including AIY and AIZ, drive positive and negative thermotaxis, respectively, in a kind of opponent process. Subsequent studies using femtosecond ablations have confirmed that paired ablation of AIY produces a cryophilic phenotype, but found that paired ablation of AIZ only abolishes negative thermotaxis but does not reveal positive thermotaxis.

The simplest way to interpret the ablation results is that AIY and AIZ are part of an opponent process that determines the rate of turning, rather than the direction of thermotaxis. Activation of AIB

and AIZ neurons promotes turning, while activation of AIY and AIA inhibit turning[25]. Taken together with the ablation results, this suggests that during negative thermotaxis, changes in temperature are detected by AFD and AWC neurons, and then integrated by the downstream interneurons to control the rate of turning. While this pathway can explain the biased random walk during negative thermotaxis, does not explain the gradual turns performed during isothermal tracking.

Further studies will be necessary to clarify the roles of downstream interneurons during each mode of *C. elegans* thermosensory behavior. These studies will likely benefit from recent advances in microscopy and calcium imaging, which should make it possible to record the activity of these neurons while the animal performs the relevant behaviors.

3.8 IMAGING OF NEURAL ACTIVITY DURING THERMOSENSORY BEHAVIORS

Ablations studies have highlighted some of the key players involved in thermotaxis and isothermal tracking, but to understand the precise roles of these neurons, it is necessary to observe their dynamic neural activity patterns in response to defined thermal stimuli and during behavior. Optical recordings of calcium activity in the AFD neuron by a FRET-based chameleon indicator in immobilized worms has confirmed that AFD indeed functions as a thermosensory neuron and clarified how thermosensory input is encoded at the first stage of the circuit[23-24]. AFD was found to respond to warming stimuli, but only above a certain temperature threshold[23]. Delivery of precisely controlled thermal stimuli revealed that a short term adaptation mechanism acting within the AFD neuron allows it to specifically sense changes in temperature, as little as 0.05°C, over a wide range of temperatures spanning 10°C[24]. The exquisite sensitivity of the AFD neuron is sufficient to conceivably support isothermal tracking to within 0.1°C as has been described[19]. For rapidly oscillating temperature inputs and abrupt temperature steps, AFD follows the changing component of the signal with a delay of < 2 seconds[24].

Furthermore, the threshold temperature above which AFD became active was found to be closely related to the setpoint temperature, T_S. Worms cultivated at 15, 20, and 25°C had an AFD response threshold of 15, 17, and 21°C. Since isothermal tracking occurs within roughly +/- 2°C of T_S, the lower end of the AFD response range is in good agreement with the temperature range in which the behavior is performed. The thermosensory and adaptation properties of the AFD neuron were shown to arise in the sensory dendrite of AFD, based on femtosecond ablations midway between the sensory endings and the cell soma[24] that spared thermosensory signals in the sensory endings but abolished them in the soma. The experimenters found that AFD responds to temperature changes with similar gain at all temperatures above the threshold temperature, which is consistent with AFD having a role in controlling both isothermal tracking and negative thermotaxis. A remaining question that apparently cannot be explained by AFD's thermosensory properties is how animals switch between isothermal tracking and negative thermotaxis, since the AFD neuron apparently encodes sinusoidal stimuli near T_S in a similar fashion to sinusoidal stimuli at temperatures >2 °C above T_S. The distinction between the temperature range for isothermal tracking and the range for negative thermotaxis may be set by the activity over another thermosensory neuron (see below).

Multiple calcium imaging studies have shown that the olfactory neuron AWC can function as an additional thermosensory input in the *C. elegans* circuit, although there are different accounts of precisely how thermal information is encoded[30,49]. One study claimed that AWC thermosensory activity deterministically reports thermosensory stimuli and contributes to negative thermotaxis[30]. Another study found that AWC responds to thermal stimulation stochastically, and response to temperature changes both above and below the cultivation temperature[49]. The differences in the manner of activation may be related to the precise thermal stimuli used to probe AWC activity. Nonetheless, AWC appears to provide an additional source of thermosensory input to the circuit, while also possibly providing an explanation for some of the outstanding phenomena that could not be explained by AFD

alone. For example, bilateral ablation of AFD weakens but does not abolish thermosensory behavior, while combined ablations of AFD and AWC results in animals with no temperature preference[30]. The activity of AWC in one study was found to be higher at temperatures that induce negative thermotaxis than at temperatures that trigger isothermal tracking, raising the appealing possibility that AWC allows animals to distinguish these two thermosensory contexts[49].

The thermosensory neuron recordings described thus far have all been performed in immobilized animals. While this preparation simplifies data collection and analysis, it provides only a partial understanding of the ways in which neurons are active during free behavior. For example, neural signals that correlated with locomotor movements of the animal cannot be effectively studied in this way. Thanks to recent technological advances, it is now possible to record calcium activity from individual identified neurons in partially immobilized and freely behaving worms. A recent study investigated calcium activity in AFD while worms freely navigated a spatial thermal gradient[28]. The investigators found that the AFD neuron encodes spatial information about the thermal gradient could in principle be sufficient to control both isothermal tracking and negative thermotaxis behavior. The authors found that AFD phase locks to the oscillations in temperature induced by undulating head swings of the animal's own movement. This means that any imbalance in the activation of AFD as a function of the phase of the animal's undulation could be used as a signal to update the heading of the animal by gradual turning to maintain alignment to isotherms during isothermal tracking. The proposed utilization of the AFD thermosensory signal in relation to the animal's own movement is a remarkable example of active sensing, and recalls examples of similar processes in complex vertebrate systems such as whisking in rodents[50]. The investigators also show that the AFD neuron activity is positively correlated with the instantaneous heading of the animal at high temperatures. When animals are heading up the gradient at high temperatures, the first derivative of temperature is positive and AFD tends to be more active. Thus, on a timescale longer than the individual undulation cycle, the activity of AFD tends to

report whether or not the current run is in a favorable direction. This means that the activation of AFD can be used to modulate the rate of reorientation and reversal events to facilitate a biased random walk down the thermal gradient. The rapid adaptation of AFD allowed the neuron to report temperature changes reliably and consistently over a wide range of temperatures above the cultivation temperature.

The thermal stimulus information encoded in the AFD neuron appears to be sufficient to control both negative thermotaxis and isothermal tracking. If the AFD neuron is indeed the sole or predominant sensory signal, then there are fascinating questions regarding the mechanisms by which the downstream circuitry decode the relevant components of the signal. Based on the description of the AFD activity in freely behaving worms, it would appear that the ideal decoding strategy would isolate the asymmetric component to drive gradual turning during isothermal tracking, and separately isolate the symmetric component to suppress reorientation. The downstream circuitry that controls isothermal tracking would isolate the asymmetric component of AFD activity, and then promote dorsal or ventral extension to gradually realign the overall heading to the isotherm. The downstream circuitry that controls negative thermotaxis circuit would isolate the symmetric component of AFD activity, and then proportionally suppress reorientation.

3.9 OPTOGENETIC MANIPULATION OF NEURAL ACTIVITY

Thanks to advances in optogenetic tools and the optical setups that are used to drive them, *C. elegans* researchers have been able to activate and inhibit individual identified neurons in freely behaving animals and observe the consequences on behavior[51-52]. In a recent study, investigators expressed the light-activated cation channel Channelrhodopsin-2 (ChR2)[51] or light-driven outward proton pump archaerhodopsin-3 (Arch) in a variety of neurons including AIY, AIB, and AWC[53]. These optogenetic tools allow spatiotemporally defined activation by 480 nm light (ChR2) and inactivation by 540 nm light (Arch). Inspired by the symmetric and asymmetric components of sensory input induced by

the worm's undulatory locomotion (discussed in previous section as it applies to AFD), the researchers drove ChR2 or Arch with temporal waveforms that were either asymmetrically locked to the phase of undulatory locomotion or symmetric with respect to the undulation.

The authors found that asymmetric stimulation of AIY promotes gradual turning. The direction of turning was dependent on whether stimulation was asymmetrically higher during the dorsal or the ventral phase of the head bending. Activation of AIY by symmetric stimulation led to a reduction in reversal events. Thus, the asymmetric and symmetric components of AIY stimulation could separately modulate gradual turning and abrupt reversals, two processes that are central to chemotaxis. Although the authors did not interpret their results in the context of thermotaxis or isothermal tracking, the results could be consistent with the overall model of these behaviors that we have described in the preceding sections. During isothermal tracking, asymmetric activation of AFD and perhaps AWC could drive asymmetric activation of AIY, which in turn would drive gradual turns to maintain alignment with the isotherm. During negative thermotaxis, unfavorable headings could activate AFD, which could inhibit AIY, which in turn could disinhibit reversals and reorientation. These experiments provide support for the view that circuits downstream of sensory neurons such as the AFD neuron can parse its information-rich encoding of thermal stimuli to drive appropriate behavioral responses.

At the other end of the circuit, optogenetics has recently been applied to alternately excite and inhibit motor neurons to control gradual bending behavior[54]. Investigators used coexpression of ChR2 as well as the light-activated chloride pump Halorhodopsin (NpHR)[55] in order to optically control the DD motor neurons that control the dorsal muscles. The authors showed that activation of these motor neurons could induce a deep ventral turn, while inhibition of these motor neurons induced a deep dorsal turn. Now that calcium imaging and optogenetics are established, one could imagine future studies taking a combined approach by first observing the activation pattern of a given neuron in some

context and then testing the sufficiency of that neuron by driving it with its own physiologically relevant activation pattern.

4 THERMOTAXIS IN DROSOPHILA LARVAE

The thermotaxis strategy employed by *Drosophila* larvae can be described as a biased random walk augmented by several strategies to enrich for turning toward favorable headings[56]. Like both *E. coli* and *C. elegans*, locomotion in *Drosophila* larvae alternates between runs and reorientations[8,57]. In a thermal gradient, the rate of reorientation is dependent on temporal changes in temperature, which is the hallmark of the biased random walk strategy. This biased random walk strategy is employed during both positive and negative thermotaxis (**Fig. 3a**). Unlike *C. elegans*, Drosophila larvae pause before each reorientation to perform one or more head sweeps[8,57] (**Fig. 3b**). These head sweeps bias the reorientation toward the preferred temperature. If the first head sweep detects a favorable change in temperature, then the animal often commits to this reorientation. If the first head sweep fails to detect a favorable change in temperature, then the animal instead performs a second head sweep in the opposite direction, and the process repeats. This strategy augments the random walk by enriching the probability that the animal reorients toward the preferred temperature.

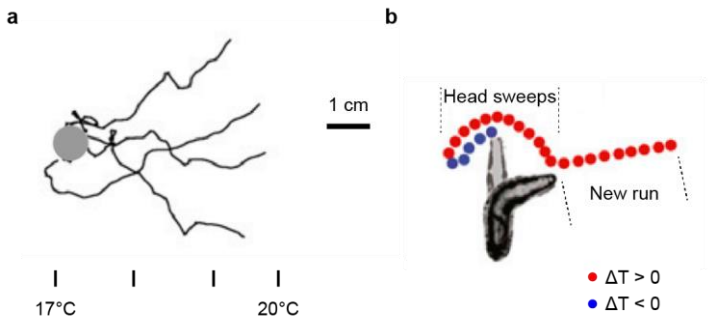

Figure 3 | Drosophila larvae perform thermotaxis using an augmented random walk strategy. a, Four *Drosophila* larvae performing positive thermotaxis. Unlike *C. elegans*, *Drosophila* larvae have a relatively stable preferred temperature at each developmental stage that does not depend on cultivation temperature. Grey circle marks starting location. Like *C. elegans*, *Drosophila* larvae extend runs when temperature changes are favorable and shorten runs when temperature changes are unfavorable. Individual trajectories are stochastic, as in a classic biased random walk, but *Drosophila* larvae incorporate some additional strategies to enhance the selection of new headings. **b,** Example head sweep sequence. Direction of initial sweep is random, but animals preferentially commit to the direction of the sweep (i.e. new run starts in that direction) or reject it depending on whether the temperature change during the sweep was favorable. If the sweep is rejected, a new sweep is conducted in the opposite direction and the process continues, with a possibility of even more sweeps depending on thermosensory feedback. In the example depicted above, a randomly selected left sweep led to an unfavorable temperature change and the animal preferentially rejected the sweep in favor of a right sweep, which led to a favorable temperature change and was preferentially converted into a new run. *Drosophila* larvae also bias the magnitude of head sweeps, so that highly unfavorable runs are aborted with large angle turns. (Figure adapted from Garrity et al.[7])

Both weathervaning and head sweeps can be seen as strategies to optimize the heading angle throughout a trajectory rather than simply controlling the rate of sudden, random reorientation. Both strategies appear to be additions to the basic biased random walk strategy observed across many organisms. However, weathervaning in *C. elegans* and head sweeps in *Drosophila* are also quite different in implementation. Head sweeps only occur before discrete turn events in Drosophila, while side to side undulations are the basis of all forward movement in *C. elegans*. Weathervaning can be viewed as biasing the direction of runs in *C. elegans*, while head sweeps bias the direction of turns in

Drosophila. Finally, weathervaning occurs in a limited temperature range around the preferred temperature, while head sweeps occur in both positive and negative thermotaxis in *Drosophila*.

In contrast to *C. elegans*, *Drosophila* larvae do not appear to adapt their preferred temperature based on thermosensory history. However, the cultivation temperature of *Drosophila* does affect their temperature preference as adults, and their preferred temperature also changes over the course of development. Early stage larvae prefer temperatures between 23 °C and 29 °C[56], while late stage larvae prefer 18 °C[58].

In *Drosophila* larvae, a number of thermosensory neurons have been identified. Terminal organ neurons and chordotonal neurons respond to negative changes in temperature[59,60]. Silencing of terminal organ neurons impairs positive thermotaxis[59]. This silencing affects all components of the *Drosophila* thermotaxis strategy, and the animal can no longer adjust its turn rate and turn direction in response to thermal stimuli. TrpA1 expressing neurons in the brain respond to positive changes in temperature, and may contribute to negative thermotaxis[61]. Calcium imaging approaches will be helpful in identifying and characterizing the major components of the downstream circuitry in the *Drosophila* thermosensory circuit.

5 THERMOTAXIS IN VERTEBRATE SYSTEMS

Thermotaxis has been observed in a number of vertebrate systems, but no quantitative study of thermotaxis behavior has been conducted[62-69]. For endothermic mammals, thermotaxis toward the preferred temperature is not as essential to survival as it is for ectotherms that must regulate body temperature by behavior alone. Nevertheless, a number of mammals have been observed to migrate toward a preferred temperature zone in a thermal gradient. Thermotaxis is particularly important for neonatal rats and hamsters, which cannot internally regulate their body temperature[65-66]. At 4-5 days post birth, these animals rely on thermotaxis to maintain optimal body temperature.

Adjustments to temperature preference over long time scales have also been documented in vertebrate systems[62]. For example, golden hamsters prefer a much lower temperature (8 °C) pre-hibernation than post hibernation (24 °C) [62,67]. These adjustments to thermotaxis set-point may reflect different biological needs at different stages of development and under different environmental conditions.

In zebrafish, Prober et al. have shown that larval zebrafish are capable of increasing locomotor activity in response to noxious thermal stimuli[70]. However, no detailed sensorimotor mapping between thermal stimuli and locomotion has been conducted. Previous studies have also characterized to a limited extent zebrafish locomotion in general and escape behavior in particular[71-73]. It is worth noting that the basic locomotor pattern of larval zebrafish differs from both *C. elegans* and *Drosophila* larvae. While *C. elegans* and *Drosophila* larvae move continuously during runs, larval zebrafish move in discrete bouts and come to rest between successive bouts. For each bout, one can measure the peak velocity, displacement and turn angle. Previous studies of zebrafish locomotion tend to view individual bouts as independent events. As we will discuss in Chapter 3, this view may be a simplification of the actual locomotor pattern of larval zebrafish, and sustained bias in turn direction across multiple movements may be an essential mechanism in zebrafish thermal navigation.

Primary thermosensory cells have been extensively characterized in vertebrate systems[74-77], but a circuit for behavioral regulation of temperature has not yet been identified. In vertebrate systems such as rodents, primates, or teleost fish, the thermosensory stimuli are detected by a set of specialized peripheral organs – the trigeminal ganglion and dorsal root ganglion (DRG). Each ganglion is a collection of somatosensory cells that respond to mechanical, chemical, proprioceptive, and thermal stimuli[75]. The trigeminal ganglion represents the face and neck of the animal, while each DRG represents one body segment. In larval zebrafish, the trigeminal ganglion is formed by 24 hours post fertilization[78-79], while the DRG emerge around 5 days post fertilization (dpf) [80-82]. Before the emergence of DRG cells, a

collection of rohon beard neurons line dorsal spinal cord and report somatosensory stimuli to the trunk and tail of the fish[82-83]. Zebrafish have a subset of relatively conserved Trp channels relative to mammals. In particular, TrpV1 has recently been shown to mediate detection of heat above 25 °C in a defined subset of trigeminal ganglion neurons[84]. In the same study, investigators used a morpholino directed against TrpV1 to show that the receptor is required for early behavioral responses to heat at 3 dpf. The knock-down effect was strongest at mildly warm temperatures including 28.5 °C and 32.5 °C but is largely overwhelmed at 34.5 °C. Although it is formally possible that another receptor mediates responses at in the more noxious temperature range, a simpler explanation is that knock-down by the morpholino is incomplete. Genetic mutants for TrpV1 will be necessary to distinguish these possibilities, as well as to extend the phenotypic analysis of TrpV1 loss of function since morpholino knock-down does not persist until behaviorally relevant larval stages such as 7-8 dpf.

At present, the lack of understanding regarding thermosensory channels, circuitry, and behavior in zebrafish stems from a paucity of behavioral assays for thermosensation or thermotaxis. In vertebrate systems as a whole, understanding of thermosensory behavior is largely limited to primary sensory cells. Behavioral strategies for thermal navigation and the circuitry that underlie these strategies have not been explored in depth. We aim to establish a framework for investigating thermotaxis behavior in zebrafish, uncover the sensorimotor mappings between temperature and locomotor elements, and model the components of navigational strategy. This represents the first quantitative analysis of thermal navigational behavior in a vertebrate system. With the optical and genetic advantages of the larval zebrafish system[85-87], a characterization of thermotatic strategy would open up many potential areas of research into the molecular and neuronal basis of thermosensation and spatial navigation.

2. Spatiotemporal control of thermal stimuli in larval zebrafish

1 INTRODUCTION

Larval zebrafish have the potential to be a powerful system for combining quantitative behavioral analysis with comprehensive imaging of neural activity. Due to the infancy of this field, however, relatively fewer behavioral paradigms have been established compared to other model organisms such as *C elegans*, Drosophila, and rodents. We have focused on establishing larval zebrafish as a system for studying thermosensory behaviors including spatial navigation and operant learning. Since thermosensory behaviors have not been extensively studied in larval zebrafish, we went through an iterative design process to obtain 1) a chamber optimized to stably deliver spatial temperature gradients and 2) a chamber optimized to deliver rapidly changing thermal waveforms.

The most challenging part of both designs was the fact that we must control the temperature of a volume of water, rather than just the surface temperature of the chamber floor as we would do for *C elegans* or Drosophila. The simple fact that fish live in water forced us to confront unwanted effects such as evaporative cooling and convection currents. Water also has an exceptionally high specific heat, more than ten times that of copper, which means that we must add or remove large quantities of heat to obtain a given change in the water temperature. In this chapter, I will present the design and characterization of two behavioral chambers that address all of these issues and facilitate the study of thermosensory behaviors in larval zebrafish.

2 DELIVERY OF SPATIAL TEMPERATURE GRADIENTS

We have developed a behavioral chamber to deliver spatial temperature gradients to freely behaving larval zebrafish (**Fig. 4a-b**). We designed the chamber to be radially symmetric so that we can

present 25 °C (neutral) in the center and 37 °C (noxious) around the edge. This gradient shape has the advantage that avoidance of noxious temperatures will naturally restrict the behavior to the interior of the chamber, away from the chamber walls which would complicate the analysis.

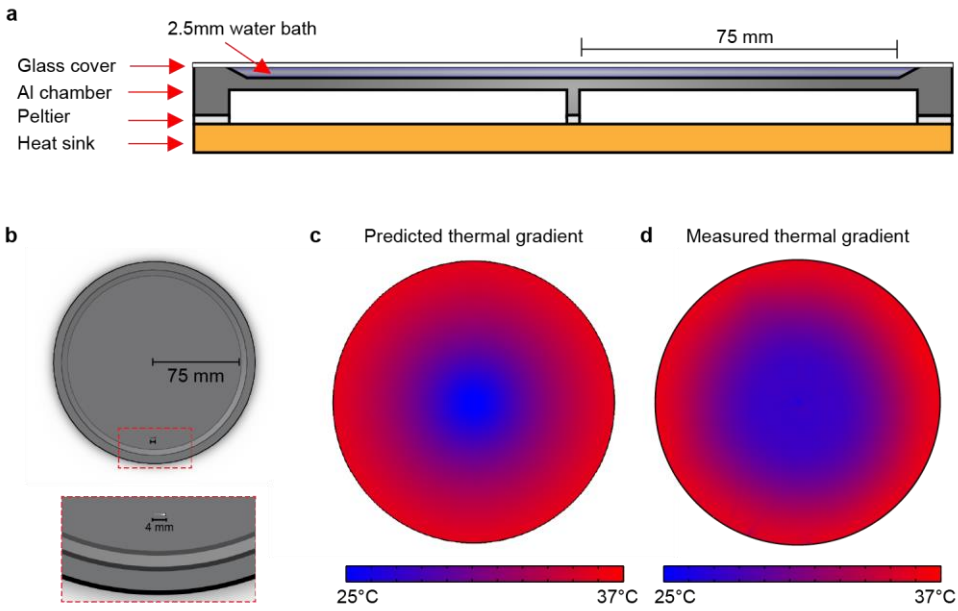

Figure 4 | A radially symmetric behavioral chamber to deliver tightly controlled, stable thermal gradients to larval zebrafish. a, Design of the radial gradient chamber. A recessed pocket 2.5 mm deep is filled with water and covered with a thin glass wafer to form a closed behavioral chamber for thermal navigation. Peltier elements, thermistors, and custom electronics mounted under the edge and center of the chamber implement a custom PID control loop to rapidly form the thermal gradient and stably maintain it within 0.1 °C. **b,** Top view of chamber, showing 7 dpf larval zebrafish for scale. **c,** Simulated steady-state thermal gradient based on finite element modeling. The model was instrumental during the design process due to its ability to quantify the dynamics of gradient formation and the shape of the steady state gradient. The model assumes firm boundary conditions of 25 °C and 37 °C and realistically models the physics of thermal conduction in the aluminum chamber, thermal conduction and convection in the water, thermal conduction in the glass cover, and convective cooling to the air above the cover. **d,** Experimentally measured steady state distribution of the thermal gradient. A thermal imaging camera (uncooled microbolometer) was used to capture an image of the surface temperature of the chamber after reaching steady state.

The dimensions of the water bath were chosen so that the thermal gradient would have a shallow slope. Using a bath diameter of 150 mm, the water bath transitions from 25 °C to 37 °C across a distance of 75 mm, yielding a slope of 0.16 °C / mm. For reference, a single swim bout of a larval

zebrafish in the gradient involves a displacement of around 4 mm. Given the slope of the radial gradient, a typical movement would lead to a temperature change of -0.64 °C to +0.64 °C, depending on the heading of the animal.

The chamber is machined from a single block of aluminum. We create a recessed cavity in the top surface of the aluminum to contain the water bath. We initially tested the chamber with the top open to the air and found that evaporation of water created two undesirable effects. Firstly, evaporation significantly reduced the bath height over the course of an experiment. Secondly, the process of evaporation leads to an effect called evaporative cooling, in which the energy required for the phase change of water is drawn from the remaining bath volume and lowers its temperature. Based on the chamber geometry, water's high heat of vaporization, and the ambient humidity, we estimate that evaporative cooling leads to roughly 7 W of heat loss across the chamber surface. Based on these observations, we decided to cover the bath using a glass wafer that is 150 mm in diameter and 0.6 mm thick. In addition to preventing evaporation, the cover has the added benefit of insulating the bath temperature from the air above the chamber, reducing thermal losses due to convective cooling by the air.

Our strategy for forming the thermal gradient relies on the physics of thermal diffusion. We clamp the edge and center temperatures of the aluminum chamber body, which establishes a set of boundary conditions for thermal diffusion. Since aluminum has a high thermal conductivity, the chamber body will rapidly form a temperature gradient between the boundary conditions. To ensure that the resulting steady state thermal gradient is linear from center to edge, we had to modify the underside of the aluminum disk to resemble a hub and spoke geometry. This ensures that the total cross sectional area at each radius along the thermal conduction path is the same. We confirmed that our design yields a linear gradient at steady state using finite element modeling (**Fig. 4c**) as well as measurements of the actual chamber temperature using a thermal imager (**Fig. 4d**).

To stably maintain the boundary conditions, and hence the thermal gradient, we implemented a closed loop feedback system. Briefly, we monitor an array of thermistors embedded around the edge and center of the aluminum chamber body, calculate feedback using a custom PID controller running on embedded hardware, and then drive peltier elements mounted to the underside of the chamber using custom electronics. Our control system is stable to within 0.1 °C.

To characterize the dynamics of gradient formation in our chamber design, we used finite element modeling (**Fig. 5**). We find that the gradient forms initially in the aluminum chamber and then transfers to the water. Both the aluminum and the water stabilize to a linear thermal gradient within 3 min. We also used our model to estimate the magnitude of convective water flow that arises due to the spatial inhomogeneity in the water temperature. Convective flow is largest during gradient formation (approximately 0.5 mm/s peak flow), but becomes negligible after the gradient has stabilized (< 0.1 mm/s).

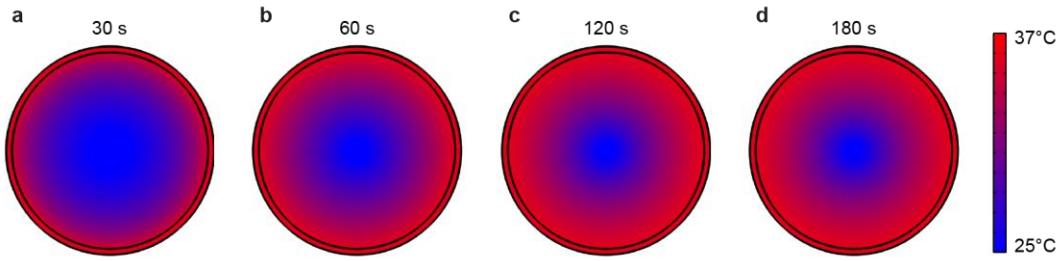

Figure 5 | Modeled dynamics of thermal gradient formation. a-d, Instantaneous temperature distribution in the gradient chamber at 30 s (**a**), 60 s (**b**), 120 s (**c**), and 180 s (**d**). The finite element model predicts that the gradient stabilizes within 3 min. Measurements at various bath locations with a thermistor were consistent with the model.

3 DELIVERY OF TIME-VARYING THERMAL WAVEFORMS

By observing navigation in the thermal gradient chamber, we can identify potential strategies that the fish might use to map thermosensory experience to motor responses. However, the gradient

chamber alone cannot distinguish whether animals use a fixed navigation strategy or whether they require sensory feedback to adapt their strategy as they traverse the gradient. To resolve these ambiguities, we developed a thermal stimulation chamber that can deliver uniform, rapidly time-varying thermal waveforms (**Fig. 6a**). The design of this chamber minimizes the response time of the entire bath volume, making it possible to deliver controlled temperature steps and sinusoidal oscillations. We have confirmed the fast dynamic performance of our design using finite element modeling and empirical measurement of the bath temperature (**Fig. 6b**) while delivering thermal steps and sine waves.

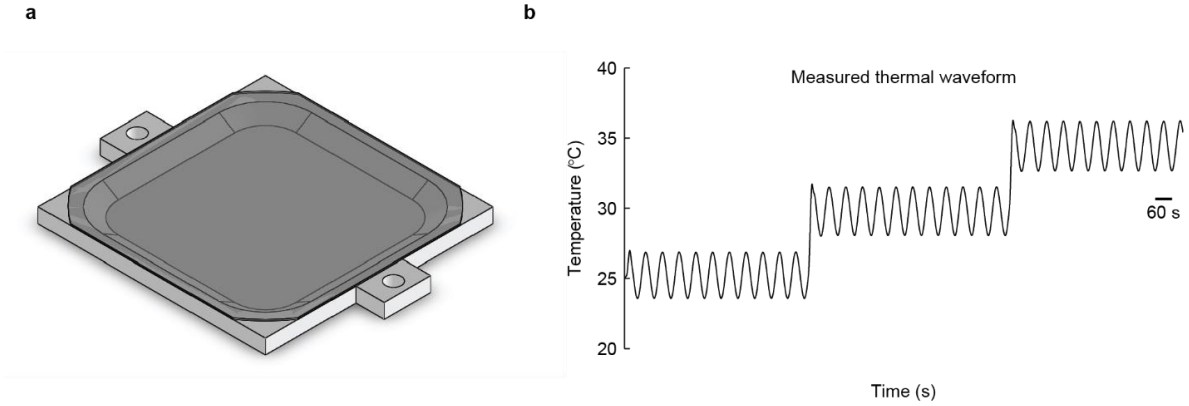

Figure 6 | Thermal waveform chamber. a, Design of the thermal waveform chamber. A recessed pocket 2.5 mm deep is filled with water and covered with a thin glass wafer to form a closed behavioral chamber for recording behavioral responses to arbitrary thermal waveforms. A powerful 400 W peltier element is mounted directly under the chamber. A thermistor reports the chamber floor temperature to custom digital electronics and a control loop establishes a firm boundary condition in the chamber floor according to the desired thermal waveform. The bath temperature passively follows the chamber floor by thermal conduction. **b,** Measured temperatures during thermal steps and sine waves.

Our approach is to establish a firm boundary condition on the bottom and sides of the chamber and an insulating boundary condition above the chamber. We use closed loop feedback at 5 Hz and a powerful 400 W peltier to rapidly adjust the temperature of the floor and sides so that they constantly track the desired stimulus waveform. We insulate the top surface of the water bath with a laser-cut 0.4

mm glass wafer. We rely upon the physics of thermal conduction to rapidly equilibrate the temperature of the bath volume to that of the floor and walls.

At steady state, the temperature of the bath volume will match the boundary temperature below. Transiently, however, the time required for the bath volume to follow the boundary temperature depends on the choice of bath height. We used finite element modeling to predict the step response time of the overall bath temperature over a range of bath heights from 1 mm to 10 mm (**Fig. 7**). Our modeling revealed that a small increase in bath height can severely slow the speed of thermal equilibration. As a point of reference, the distance between the dorsal and ventral surface of a larval zebrafish at 7 dpf is 0.5 mm. To determine whether constraining the animal's range of vertical travel would impact behavior, we assayed the effect of bath height on spontaneous larval locomotion over a height range of 1 mm to 10 mm. We found that locomotion appeared normal in bath heights from 2.5 mm to 10 mm. Bath heights between 1.5 mm and 2.0 mm led to mild perturbations in behavior, such as decreased displacement per bout, and a bath height of 1 mm severely perturbed locomotion, causing frequent escape bouts. Our results suggest that larval zebrafish require > 2 mm of vertical space to maintain normal locomotion, so we decided to use a bath height of 2.5 mm to optimize thermal response time while minimizing behavioral disruption.

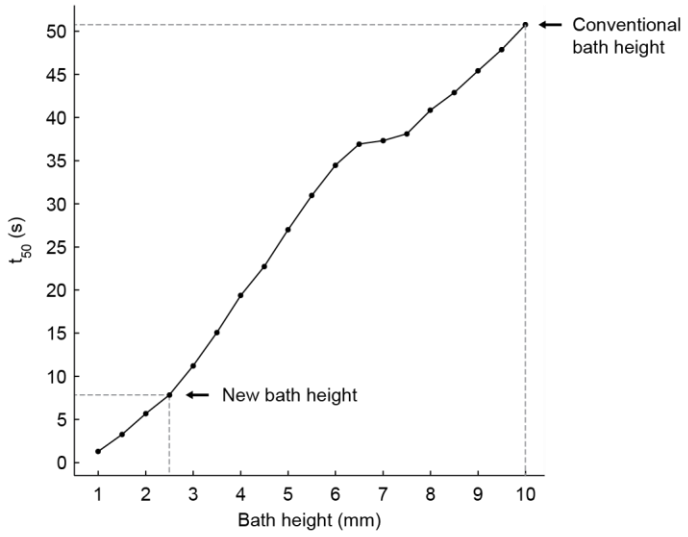

Figure 7 | Predicted step response time as a function of bath height. Time to reach half maximal response, t¬50, is plotted as a function of bath height in the thermal waveform chamber. Behavioral chambers in the lab typically use a bath height of 10 mm, which is 20 times the height of a 7 dpf zebrafish. We selected a bath height of 2.5 mm to minimize the lag between the chamber floor temperature and the bath temperature, subject to the constraint that zebrafish locomotion is perturbed at a bath height of 2.0 mm or less. Note that the plot deviates from a straight line due to the emergence of convective flows as bath height increases.

Another potential concern about heating from the bottom of the chamber is that we might generate convection currents in the water. When a volume of water is heated from below, the water on the bottom expands as it heats until it can no longer support the colder, denser water above it. The hot and cold water exchange places with each other by forming convective flow loops. This phenomenon would not occur during cooling from the bottom since the hotter, lighter water is on top of the colder, denser water. Larval zebrafish are extremely sensitive to fluid flow, and hence we must be careful to avoid introducing convective water flow as an unintended stimulus. Convective flows would be of particular concern in our interpretation of the sinusoidal thermal stimulus, since they would only occur during the heating phase and hence behavioral responses during heating might be driven by flow, rather than thermosensory circuitry.

Our analysis of bath height has revealed that a shallow bath volume is essential to avoid convective currents in the water. At a bath height of 2.5 mm, the viscous damping force of the water exceeds the gravitational force of the cooler, denser upper layer of water and so we avoid convective currents (**Fig. 8a**). We have confirmed the lack of convective forces in our chamber by tracking a paralyzed fish during our thermal stimulation protocol. By contrast, a 10 mm bath height has large convective flows (**Fig. 8b**). This analysis explains why multiple behavioral chambers in the lab using a 10 mm bath height have encountered problems with convective flows. Our finite element analysis is consistent with analytical results of Rayleigh-Bénard Instability. Assuming a 1°C temperature difference between the top and bottom of the water bath volume, our 2.5 mm chamber design has a Rayleigh number < 10, whereas a typical 10 mm zebrafish behavioral chamber has a Rayleigh number > 1000, where convection begins to overwhelm conduction.

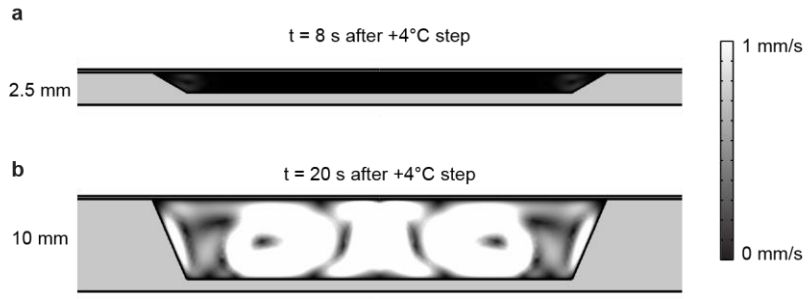

Figure 8 | Shallow bath volume is essential to avoid convective water currents. a-b, Instantaneous magnitude of water flow in the thermal waveform chamber after a +4 °C step in the chamber floor temperature. With a 2.5 mm bath height (**a**), temperature propagates from the chamber floor by conduction rather than convection, whereas with a 10 mm bath height (**b**), large convective flows can be seen.

An extensive characterization of our behavioral chambers by both modeling and empirical measurements has been critical to optimizing the response time and stability of the thermal stimuli we deliver to the larval zebrafish. Many potentially confounding factors such as convection and evaporative cooling have not been considered in traditional designs of behavioral chambers for zebrafish. For

example, a typical behavioral apparatus with a bath height of 10 mm can severely retard thermal equilibration and generate large convective currents. Our theoretical and empirical approach has allowed us to design and construct two behavioral chambers that maximize the speed and stability of thermal stimulus delivery while minimizing interference from other sensory modalities.

4 CONCLUSION AND DISCUSSION

We have developed a pair of complementary behavioral chambers for studying navigation in spatial temperature gradients as well as behavioral responses to time-varying thermal stimuli. Our radial gradient chamber allows us to test the ability of zebrafish to restrict to a preferred temperature zone when presented with a radially symmetric thermal gradient from 25 °C to 37 °C. Our thermal waveform chamber allows us to test how fish respond to thermal stimulation in the absence of movement-induced sensory feedback.

Natural extensions of this work would be to construct alternative gradient shapes such as a rectangular linear gradient, or to expand the range of temperatures to include positive and negative thermotaxis. We are also collaborating with a post-doc in the lab, Martin Haesemeyer, to develop a laser-based setup to deliver arbitrary thermal stimuli to freely swimming larval zebrafish. We believe that our peltier-based approach has the advantage of higher accuracy due to the closed loop control of the chamber temperature. On the other hand, the speed of the peltier-based setups is limited by thermal conduction in the water from the chamber floor to the fish. The laser-based approach has the advantage of higher speed because the laser can directly heat the column of water containing the fish as well as the tissue of the fish itself.

5 METHODS

Closed loop temperature control

The radial gradient was controlled by 16 feedback loops. One of these feedback loops maintained the center of the chamber at the 25 °C while the remaining 15 feedback loops held the perimeter of the chamber at either 25 °C or 37 °C. Local temperature measurements are obtained by miniature thermistors (GE Sensors) attached to the aluminum chamber body. The analog thermistor signals were collected into four groups and assigned to one of four microcontrollers (PJRC). The microcontrollers sampled the analog signals at 5 Hz and calculated feedback based on the proportional and integral terms of a custom PID controller. Each PID controller channel generated a pulse width modulated (PWM) output and a direction output, both of which were connected to a 3A motor driver (Texas Instruments) to drive a 26 W peltier element (CustomThermoelectric). The peltier elements were mounted under the chamber near their corresponding thermistor. Thermal contact between the peltiers and the aluminum chamber was optimized using 0.5 mm thick compressible thermal pads (t-Global Technology).

The control strategy for the thermal waveform chamber was very similar, except that the 400 W peltier required a higher current driver (Pololu) and a high capacity 12 V power supply (Corsair). The thermal image of the steady state temperature distribution of the radial gradient chamber was obtained with an uncooled microbolometer (Xenics) and CameraLink framegrabber (National Instruments).

Finite element modeling of chamber physics

Finite element modeling was performed using Comsol Multiphysics v4.3.

3. Quantitative behavioral analysis of thermal navigation in larval zebrafish

1 ABSTRACT

Animals navigate the world in response to sensory stimuli. In the case of thermal stimuli, navigation allows animals to maintain a preferred body temperature and avoid noxious temperatures. Despite pioneering studies in invertebrate model systems, strategies for thermal navigation in vertebrates is poorly understood. We have established a system for studying thermal navigation in larval zebrafish. We show that zebrafish can navigate a thermal gradient and restrict their locomotor trajectories to a preferred temperature zone without relying on other sensory inputs such as vision or mechanosensation. Using a high speed imaging system and real-time fish tracking software, we can resolve individual movements and analyze how the various components of a movement event are modulated by distinct aspects of thermosensory experience. We find that high absolute temperature reduces the dwell time between movements, increases displacement, and increases turn magnitude. On the other hand, we find that relative increases in temperature drive larger turn magnitudes and an enhancement of turning in a preferred direction. We assayed the same sensorimotor relationships with purely temporal thermal stimulation in the absence of a spatial gradient and found that absolute and relative temperature modulates the various components of a movement event in the manner that we would predict from the gradient behavior. We propose a model for zebrafish thermal navigation that hinges on maintaining a preferred direction and modulating the direction and magnitude of turns in response to relative temperature changes. We will test the merits of this model in Chapter 4.

2 AN ASSAY FOR THERMAL NAVIGATION IN LARVAL ZEBRAFISH

We have developed an assay for thermal navigation in larval zebrafish. Briefly, we track the position and heading of individual 7-8 dpf larval zebrafish using high speed infrared imaging while animals navigate a large circular chamber in two thermosensory conditions in the dark. We perform our assays in darkness so that we can avoid any confounding contribution to navigation by visual cues and hence can interpret any navigation decisions exclusively in terms of thermosensory information and motor history. After observing baseline locomotor behavior for 30 min while holding the entire chamber at an innocuous temperature (25 °C), we clamp the edges at a noxious temperature (37 °C) and assay thermal restriction for 30 min in the resulting stable thermal gradient (see Chapter 2 for device characterization). We ran our assay on 20 larval zebrafish at 7-8 dpf to obtain a dataset of over 50,000 movement events under two contrasting conditions (Table 1).

Table 1 | Summary of the thermal navigation dataset.

Condition	Movement events (pooled across 20 fish)
Baseline (25 °C)	24,720
Thermal gradient (25 °C → 37 °C)	26,520
Total	51,240

When we compared the trajectories of larval zebrafish during the baseline condition and during thermal gradient presentation, we observed thermal restriction during the gradient that clearly differed from the baseline localization pattern. The behavior of a representative 7 dpf larval zebrafish in the baseline and gradient conditions is shown in **Fig. 9**. Analysis of the trajectories of individual fish showed that this thermal restriction is a dynamic steady state, in which animals repeatedly wander away from the center during the course of the assay but reliably change course before reaching the noxious extremes (see **Fig. 9c** for an example). This situation is ideal for analyzing the navigation strategy

underlying thermal avoidance, because we obtain many avoidance trajectories within and across fish with which to build our model.

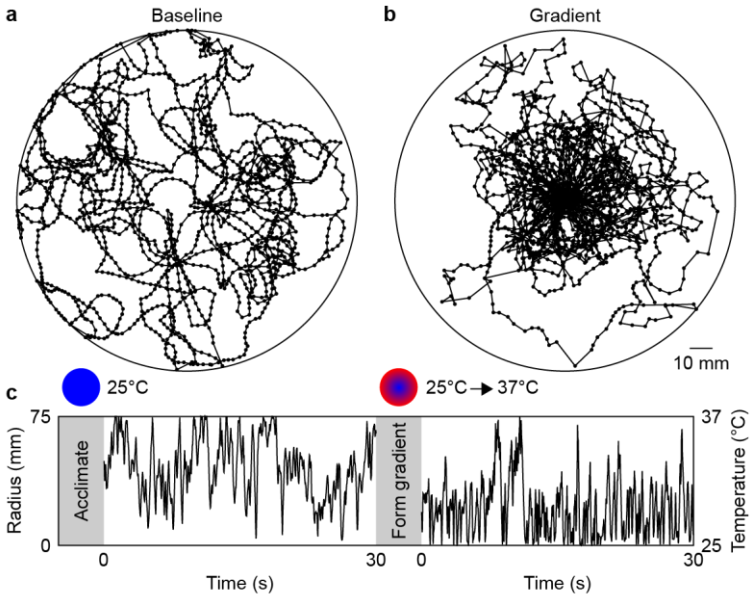

Figure 9 | Representative behavior during the thermal navigation assay. a, Trajectory of a 7 dpf larval zebrafish during a 30 min baseline period in which the entire chamber is held at 25 °C. An acclimation period of 5 min precedes the baseline period, and is excluded to avoid handling artifacts introduced by loading the fish into the chamber. **b,** Trajectory of the same animal during a 30 min gradient period in which the chamber temperature increases radially from 25 °C in the center to 37 °C at the edges. A gradient formation period of 5 min precedes the gradient period, and is excluded from analysis since the stimulus is changing during this period.

To quantify the thermal restriction, we measured the distribution of each fish along the radial axis of the chamber in both conditions. Animals showed thermal restriction to temperatures below 31 °C, in contrast to the baseline condition where they distributed uniformly across the chamber (**Fig. 10a-b**). All animals analyzed showed robust thermal restriction (**Fig. 10c**), with a highly significant reduction in the mean radius between the 30 min baseline and gradient conditions ($p < 5.6 \cdot 10^{-22}$, 1-way ANOVA). Since all 20 animals in this dataset achieved thermal restriction at a relatively similar level, we computed the overall radial distribution based on the entire population of 20 fish in the baseline and gradient conditions (**Fig. 11**). The population data confirm that larval zebrafish can perform thermal

navigation in a radial thermal gradient in darkness, using only thermosensory cues, effectively transforming a uniform baseline localization pattern into a thermally restricted pattern with enrichment below 31 °C and underrepresentation above 31 °C.

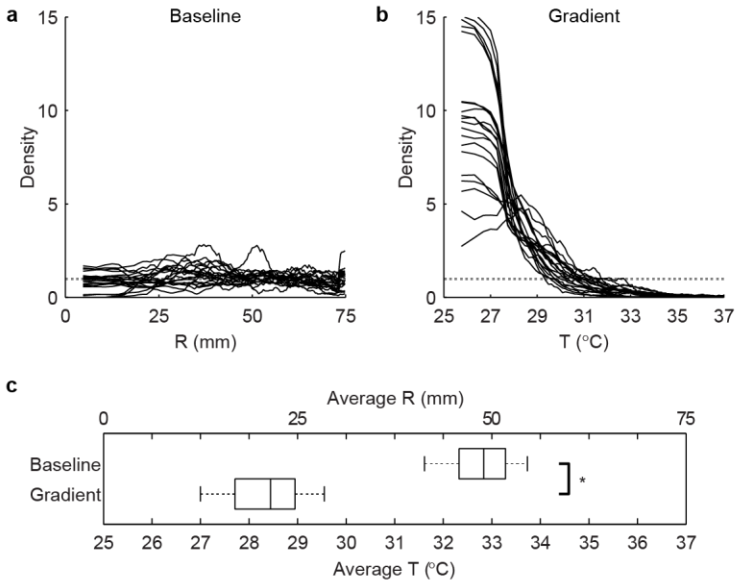

Figure 10 | Comparison of radial distributions of all fish in baseline and thermal gradient
a-b, Individual distributions of 20 larval zebrafish along the radial axis of the chamber during the 30 min baseline period (**a**) and 30 min gradient period (**b**). Dotted gray line indicates expected density assuming uniform coverage of the chamber. **c,** Box plots summarizing the average radial position (R) of the same 20 fish during the baseline and gradient conditions, as well as the average temperature (T) in the gradient condition. The difference in the means between the two conditions is highly statistically significant ($p < 5.6 \cdot 10^{-22}$, 1-way ANOVA).

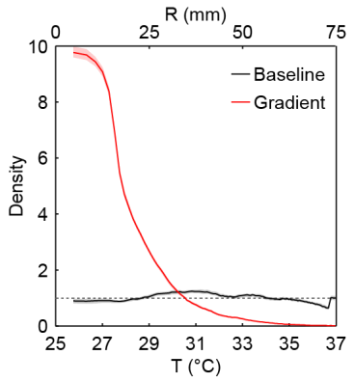

Figure 11 | Population mean distributions in baseline and thermal gradient. Mean radial distributions of entire dataset, obtained by pooling movement events of all 20 zebrafish. Shaded regions indicate bootstrapped 95% confidence interval of the mean. Dotted gray line indicates expected density assuming uniform coverage of the chamber.

In this chapter, we will show that larval zebrafish locomotion can be understood as a series of discrete movement events with four components, which we refer to as dwell time, displacement, turn magnitude, and turn direction. We show that these four components are chosen stochastically, and establish their probabilistic distributions during the baseline condition. We then ask whether absolute temperature and relative changes in temperature, two distinct aspects of thermosensory experience, have any effect on how fish stochastically select the four components of a movement event. Using two complementary quantitative approaches, kernel density estimation (KDE) and multiple linear regression, we will show that each of the four components of movement is related to one or more specific aspects of thermosensory experience. The sensorimotor transformations established in this chapter will form the basis of our model for thermosensory navigation. In the following chapter, we will use behavioral simulations to test the ability of this model to explain zebrafish thermal navigation.

3 QUANTIFYING THE COMPONENTS OF LARVAL LOCOMOTION

In order to dissect the behavioral strategies employed by larval zebrafish during thermal navigation, we developed real-time fish tracking software that records the position and heading of the

animal at 500 Hz (**Fig. 12**). Larval zebrafish move in discrete movement events that are characterized by a brief heading oscillation (**Fig. 12c**) followed immediately by a rapid change in position (**Fig. 12b**), after which animals glide to a stop at a new location in the chamber with a new heading. We define a movement event whenever either the rate of change of position or the power of the heading oscillation (AC-filtered at ~50 Hz) exceeds a threshold.

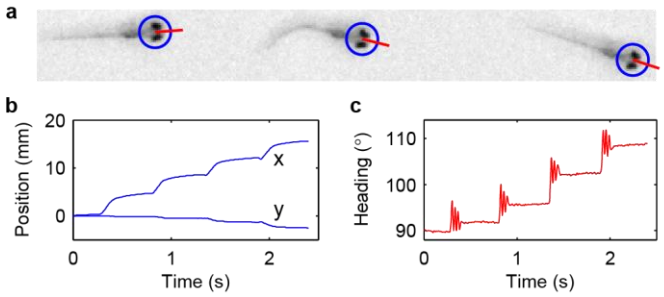

asd

Figure 12 | An automated fish tracker that allows larval trajectories to be parsed into discrete movement events. a, Real-time fish tracker tracking the position (blue circle) and heading (red line) of a larva before (left), during (middle), and after (right) a single movement event. Zebrafish are illuminated with invisible 950 nm light and tracked at 500 frames per second by custom C# software. **b,** Cartesian coordinates of fish tracked automatically by the software. The head position changes abruptly with each movement event, and then glides to a stop at a new location in the chamber. **c,** Heading angle obtained from automated tracker. Transient oscillations are induced by movement events. An automated movement decoder algorithm identifies these individual movement events and extracts the four components that characterize the movement (see **Fig. 13**).

We next sought to break down each movement into a set of locomotor components that could be separately characterized but that together would fully define the trajectory of an animal moving in the gradient. We chose to decompose each movement into its dwell time, displacement, turn magnitude, and turn direction (**Fig. 13**). We define the dwell time of a given movement as the duration of time that the animal occupied its previous position in the chamber before generating the movement. We define the displacement of a movement as the distance between the animal's position before and after the movement event. We measure the turn angle of a movement as the difference in angular heading before and after the movement, but then we decompose the turn angle into a turn magnitude,

which we define as the absolute value of the turn angle, and a turn direction, which we define as the sign of the turn angle (i.e. -1 or 1, left or right). Thus, our analysis framework breaks down each movement X into four probabilistic components, X = [dwell time, displacement, turn magnitude, turn direction]. Our decision to use these four components is not arbitrary. There are a limited number of ways to specify a movement event that can fully define the overall trajectory of an animal. Only slight variations are possible while still satisfying this goal. For example, we could have defined a movement rate as a frequency in Hz instead of defining a dwell time in seconds. These alternative formulations essentially encode the same information but as reciprocals of each other. We chose to work with dwell time because of its probability density function is bounded to a smaller interval and numerically easier to work with than frequency, but similar conclusions would be reached using frequency. Similarly, there is a small amount of flexibility in the representation of reorientation. We could have chosen to work with turn angle directly, which would have reduced the analysis to three components. However, we found that turn magnitude and turn direction were differently modulated by thermal experience, and so it made more sense to characterize these effects separately. Dissociating turn angle into magnitude and direction may also be more closely related to how these events are generated in the brain, with distinct circuit elements modulating the magnitude of turns and selecting the direction in which to turn.

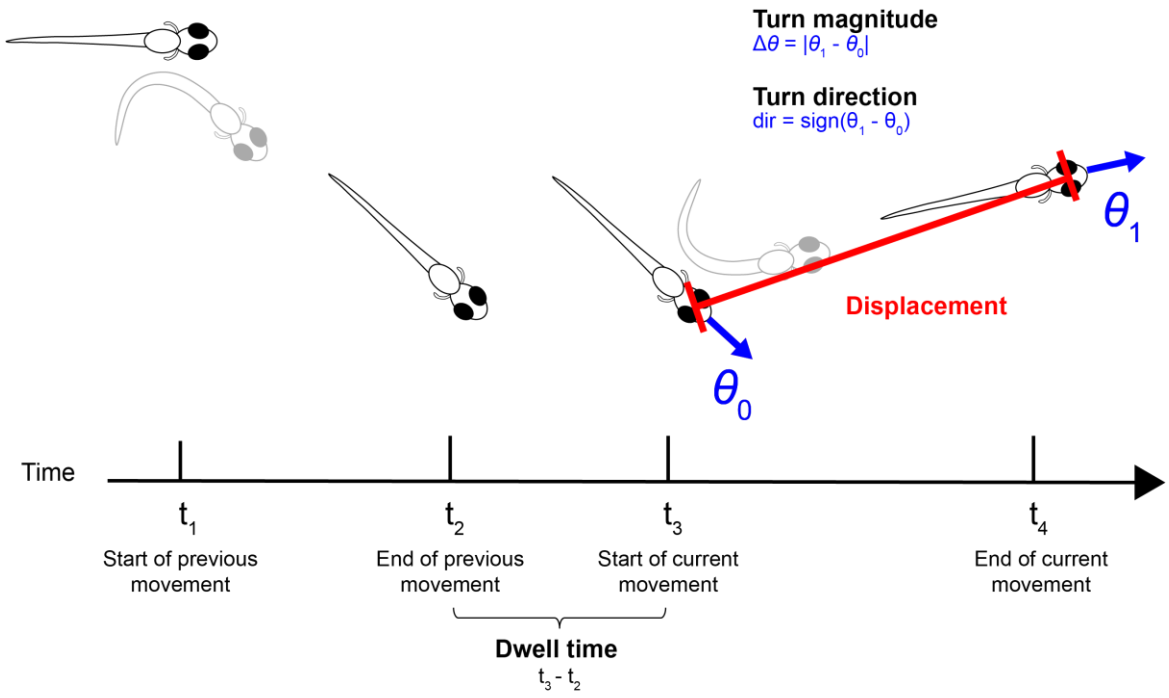

Figure 13 | Zebrafish movement events can be broken down into dwell time, displacement, turn magnitude, and turn direction. Dwell time is defined as the time that the animal remains at rest after arriving at a given location before generating a new movement event. Displacement is the distance traveled by the tracked point (the head of the animal) before and after a movement event. Turn magnitude is the absolute value of the heading change before and after a movement event. Turn direction is the sign of the heading change before and after a movement event.

To characterize the probabilistic nature of larval movement at ambient temperature in darkness, we measured the probabilistic distributions of each of the four components of a movement event using our large baseline dataset consisting of 24,720 movement events (**Fig. 14**). We find that dwell time is stochastically selected around a mean of about 1 second. Typical displacements are between 0-5 mm (for reference, the body length of a 7 dpf larva is about 4 mm). Turn magnitude varies over a wide range, with turns up to around 90° in baseline conditions. Note that a peak at 0° reflects swim events that are relatively straight, while a shoulder above around 15° reflects turn events. Nevertheless, we find that events that might be called swims and turns are part of a continuum of reorientation angles and are not cleanly resolvable as distinct categories of movement. In our analysis framework, we treat turn

magnitude as a continuously varying quantity and simply ask whether this quantity can be shifted toward larger or smaller values as a function of thermosensory experience. In the future, it may be of interest to test whether information about tail deflection (e.g. angular velocity, peak deflection angle) would cleanly resolve two subsets of movement events that could be called swims and turns. For now, we will focus on the first order question of whether absolute and/or relative temperature affect turn magnitude at all. Finally, we measure the overall probability of selecting a left or right turn. Averaged over the population data, these probabilities are clearly matched at an even 50/50 during baseline.

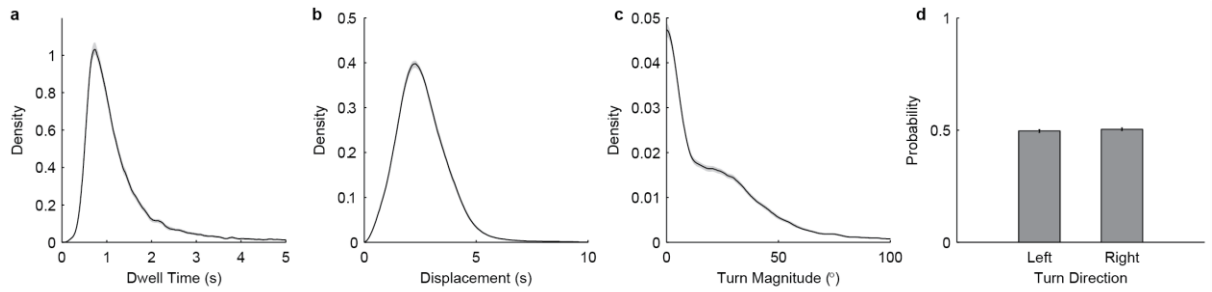

Figure 14 | Population average locomotor distributions in the baseline condition. a-c, Probability density functions for dwell time (**a**), displacement (**b**), and turn magnitude (**c**). **d,** Probability of left and right turns. Movement events were pooled across all 20 fish during baseline conditions. Error bars represent bootstrapped 95% confidence intervals of the mean.

We also investigated how stereotyped the distributions of each locomotor component are when measured within individual fish (**Fig. 15**). We find that dwell time and turn magnitude are quite similar across all 20 animals. Displacement is similar for a majority of animals, but it is interesting to note that there are a couple of individuals that show higher or lower average displacements than their siblings. We could hypothesize that this variability could be explained by slight differences in developmental stage, feeding status, or overall fish health. Since every fish in the dataset showed good thermal restriction in the assay, this variability in the overall range of displacement values does not seem to adversely affect thermal navigation. Lastly, we find that the turn direction bias in individual fish is distributed around 50% but with some variance. Larval zebrafish at 7-8 dpf appear to show moderate

handedness. Nevertheless, we will show later that turn direction bias is not a fixed quantity, but can in fact depend upon sensory inputs.

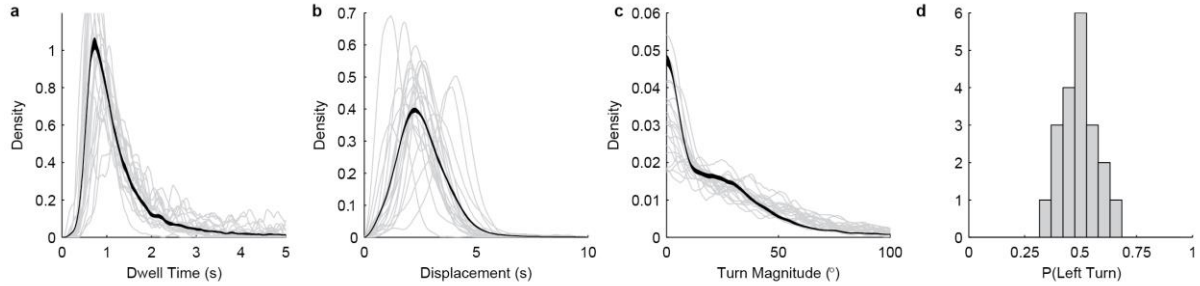

Figure 15 | Individual locomotor distributions in the baseline condition. a-c, Probability density functions for dwell time (**a**), displacement (**b**), and turn magnitude (**c**) in each of the 20 larval zebrafish in the dataset. Population mean distributions are shown for reference (black curves). **d,** Distribution of P(Left Turn), the probability of left turn, across the population of 20 fish.

4 RELATING COMPONENTS OF MOVEMENT TO THERMOSENSORY EXPERIENCE

4.1 RATIONALE

To understand how locomotion is affected by thermosensory experience, we will analyze correlations between each of the components of movement defined in the previous section and two distinct aspects of thermosensory experience. One aspect of thermosensory experience that we will consider is absolute temperature (T), which we define as the temperature the fish experienced before it generated a given movement event (i.e. the temperature experienced between times t_2 and t_3 in **Fig. 13**). The other aspect of thermosensory experience that we will consider is relative changes in temperature (ΔT) experienced during the preceding movement (i.e. the temperature change experienced between times t_1 and t_2 in **Fig. 13**). For each component of movement, we will ask: given that the fish is currently at T, having just experienced a given ΔT, what is the expected value for this component of the movement event? We will attempt to answer this question using two complementary quantitative

approaches. Firstly, we will use kernel density estimation (KDE) to measure the joint distribution of (T, ΔT, X), where X is one of the four components of movement. This will allow us to compute the conditional expectation of X given T and ΔT, i.e. $E(X \mid T, \Delta T)$. Secondly, we will use multiple linear regression to estimate the value of X, using T and ΔT as predictors. This approach is complementary to measuring the actual distributions with KDE because linear regression constrains the possible to outcomes to simple linear relationships that can be tested for statistical significance and readily interpreted. By comparing the results of KDE and linear regression, we can evaluate whether the inferred linear relationships are overly simplistic or adequately capture the relationships measured by KDE. As a control, we can test the same relationships in the baseline condition, where formally we will replace T, ΔT by the corresponding values of R, ΔR to facilitate comparison between conditions (see **Fig. 17** for correspondence between T, ΔT and R, ΔR). Consideration of the baseline condition also led us to discover an unexpected involvement of motor history (specifically, previous displacement) on current movements. With respect to thermosensory input, we will ultimately conclude that two components of movement are modulated by T, one component of movement is modulated by ΔT, and one component is modulated by both T and ΔT.

4.2 Displacement

We measured the relationship between displacement and T and ΔT in the baseline condition (**Fig. 16a**) and the gradient condition (**Fig. 17a**) using KDE as described in the previous section. Unexpectedly, we found that the ΔR of the previous movement (the proxy for ΔT in the baseline condition) seemed to modulate the displacement of the next movement (**Fig. 17a**). Based on a naïve interpretation of this data, we would be led to conclude that whenever the preceding movement brings the animal 6 mm closer or further away from the center (ΔR = ±6 mm, corresponding to ΔT = ±1 °C during gradient condition), the displacement of the next movement will be elevated. This was initially surprising to us

given that the preceding movement does not generate a thermal stimulus in the baseline condition. We realized, however, that the Δ*R* of the preceding movement is closely related to displacement of the previous movement (**Fig. 18**, correlation coefficient = 0.55). Upon further analysis, we found that the dependence of current displacement on the Δ*R* can be entirely accounted for by the autocorrelation of displacement between adjacent movements (**Fig. 19**). Unlike previous displacement, we found that previous dwell time, previous turn magnitude and previous turn direction are not correlated with *R* or Δ*R* (maximal correlation coefficient ≤ 0.1). We conclude that the displacement component of motor history must be taken into account in analysis of larval zebrafish thermal navigation, and have included this additional component (*displacement*$_{-1}$) as a predictor for the components of current movement in all our subsequent analysis (see below).

We used multiple linear regression to obtain linear models that relate the current displacement to *R*, Δ*R*, and *displacement*$_{-1}$. We then used the regression model to predict displacement as a function of *R*, Δ*R*, and *displacement*$_{-1}$for the baseline condition (**Fig. 15b**) and as a function of *T*, Δ*T,* and *displacement*$_{-1}$ for the gradient condition (**Fig. 16b**). The regression model closely recapitulates actual thermosensory relationships we obtained by KDE in both baseline (**Fig. 15**) and gradient **(Fig. 15**) conditions.

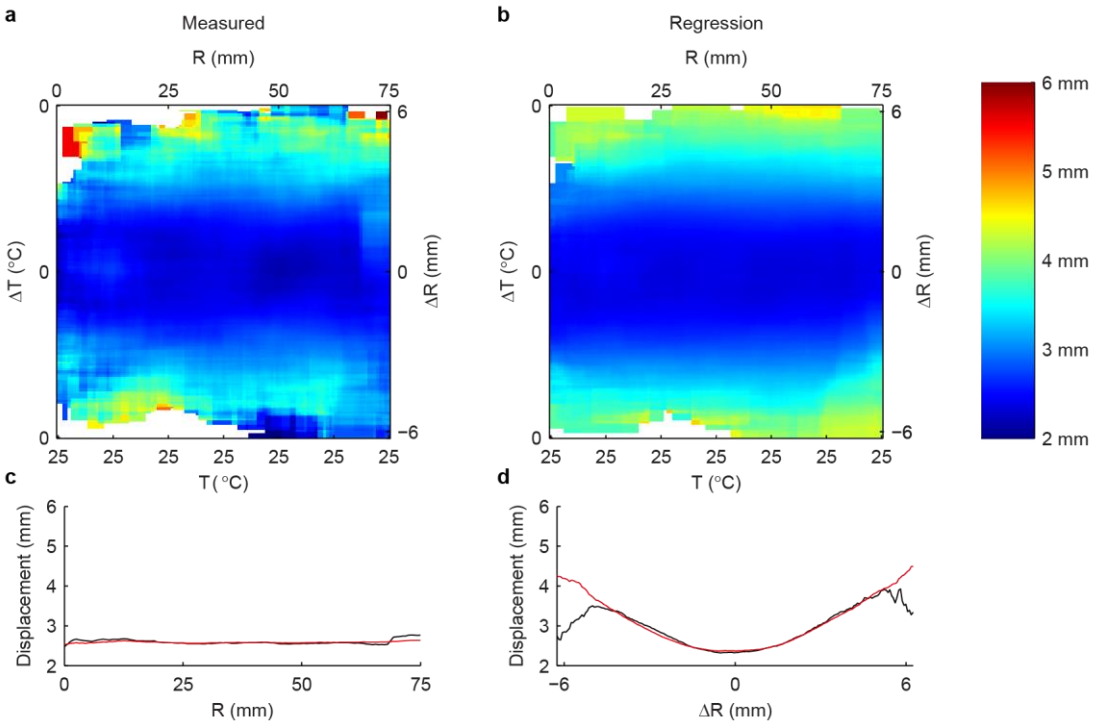

Figure 16 | Relationship between *R*, *ΔR*, and displacement in the baseline condition. a, Conditional expected value of displacement given *R* and Δ*R*. **b,** Predicted value of displacement using the linear regression model in **Table 2**. **c-d,** Estimated displacement by KDE (black line) and regression (red line) as a function of *R* (**c**) and Δ*R* (**d**).

Table 2 | Linear regression model for displacement in baseline condition.

Displacement ~ 1 + ΔR + *Displacement*$_{-1}$

Term	Estimated Coefficient	p-value
Intercept	1.458 ± 0.020	$< 1.0 \cdot 10^{-20}$
ΔR	0.129 ± 0.026	$5.2 \cdot 10^{-7}$
Displacement$_{-1}$	0.480 ± 0.007	$< 1.0 \cdot 10^{-20}$

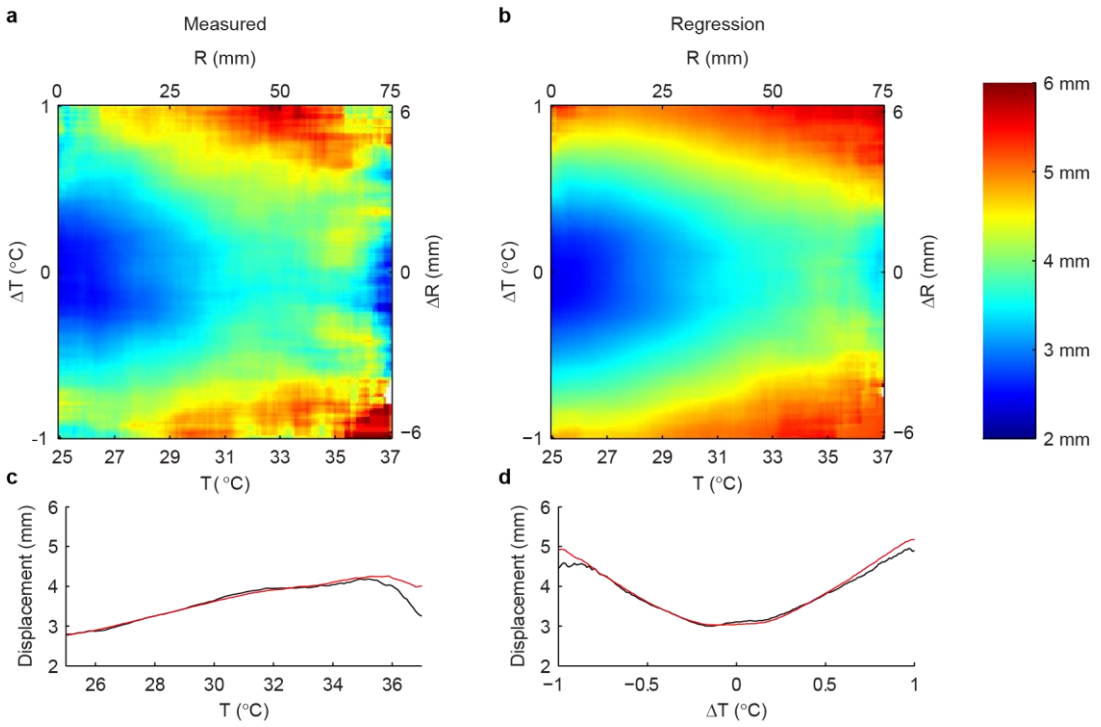

Figure 17 | Relationship between *T*, *ΔT*, and displacement in the gradient condition. a, Conditional expected value of displacement given *T* and Δ*T*. **b,** Predicted value of displacement using the linear regression model in **Table 3**. **c-d,** Estimated displacement by KDE (black line) and regression (red line) as a function of *T* (**c**) and Δ*T* (**d**).

Table 3 | Linear regression model for displacement in gradient condition.

$Displacement \sim 1 + T + \Delta T + Displacement_{-1}$

	Estimated Coefficient	p-value
Intercept	1.410 ± 0.023	$< 1.0 \cdot 10^{-20}$
T	0.081 ± 0.004	$< 1.0 \cdot 10^{-20}$
ΔT	0.122 ± 0.022	$6.7 \cdot 10^{-8}$
$Displacement_{-1}$	0.495 ± 0.006	$< 1.0 \cdot 10^{-20}$

A comparison of the terms and coefficients in **Table 2** and **Table 3** shows that the previous displacement has the largest and most significant effect on current displacement in both the baseline and gradient conditions. Specific to the gradient condition, *T* has a small but significant effect on current displacement. There is also a shared effect of Δ*R* (Δ*T*) in both conditions, but the effect size is small (i.e. only changes displacement by ~0.1 mm over a typical range of Δ*T* values) and probably unrelated to temperature since it also occurs in the baseline. By convention, our regression models and tables

include all terms that were found to have a p-value of < 0.05, but we display some terms in gray if the effect size was small or not highly significant (p > 1e-5) and therefore might not represent a real relationship.

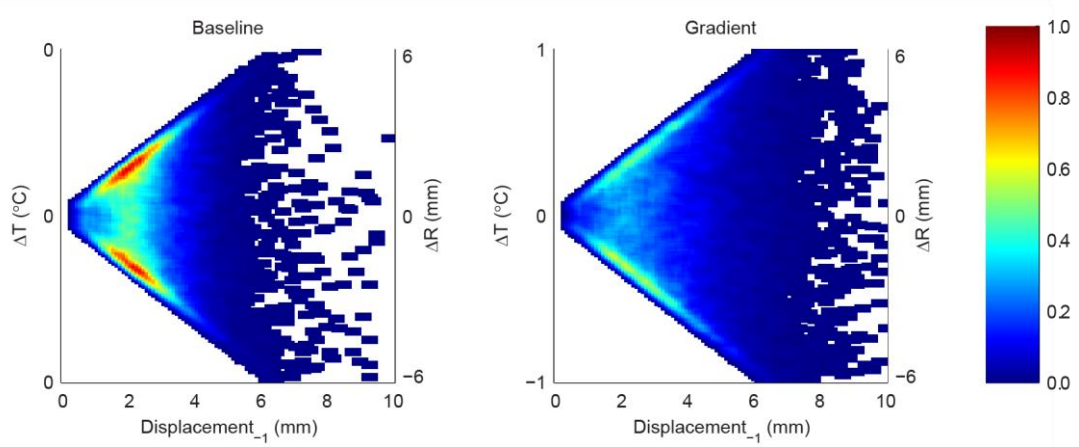

Figure 18 | Correlation between Δ*R*/Δ*T* and previous displacement. Joint probability density function for two interdependent properties of the previous movement. The Δ*R* of the previous movement and the previous displacement always obey $|\Delta R| \leq \text{Displacement}_{-1}$, with equality in the case that the previous movement was heading straight outward or inward. The same interdependence applies in the baseline and gradient conditions and shows that the effects of Δ*R* or Δ*T* can only be understood after carefully controlling for the effect of the previous displacement. Movement events were pooled from all 20 fish.

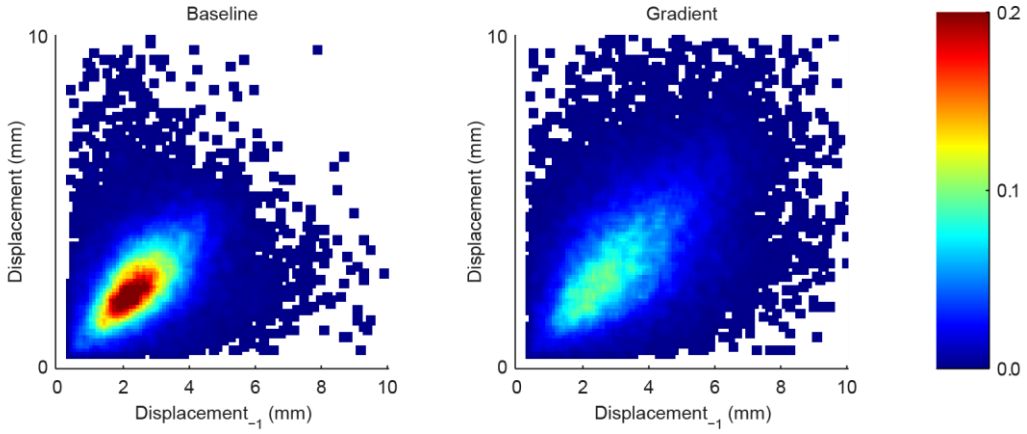

Figure 19 | Autocorrelation of displacement. Displacement of the previous movement (Displacement$_{-1}$) strongly determines the displacement of the next movement in the baseline (left) and gradient (right) conditions. Movement events were pooled from all 20 fish.

We also devised a way to assess the relationship between T, ΔT, and displacement for a clean subset of the data where ΔT and previous displacement are uncorrelated (**Fig. 20a**, **Fig. 21a**). We find that for this restricted subset of the data, we do not observe systematic modulation of displacement by R or ΔR in the baseline condition (**Fig. 20**), but we continue to see modulation of displacement by T in the gradient condition (**Fig. 21**). This analysis supports the conclusions that we obtained above, but with a simpler analysis that does not require controlling for an additional correlated predictor.

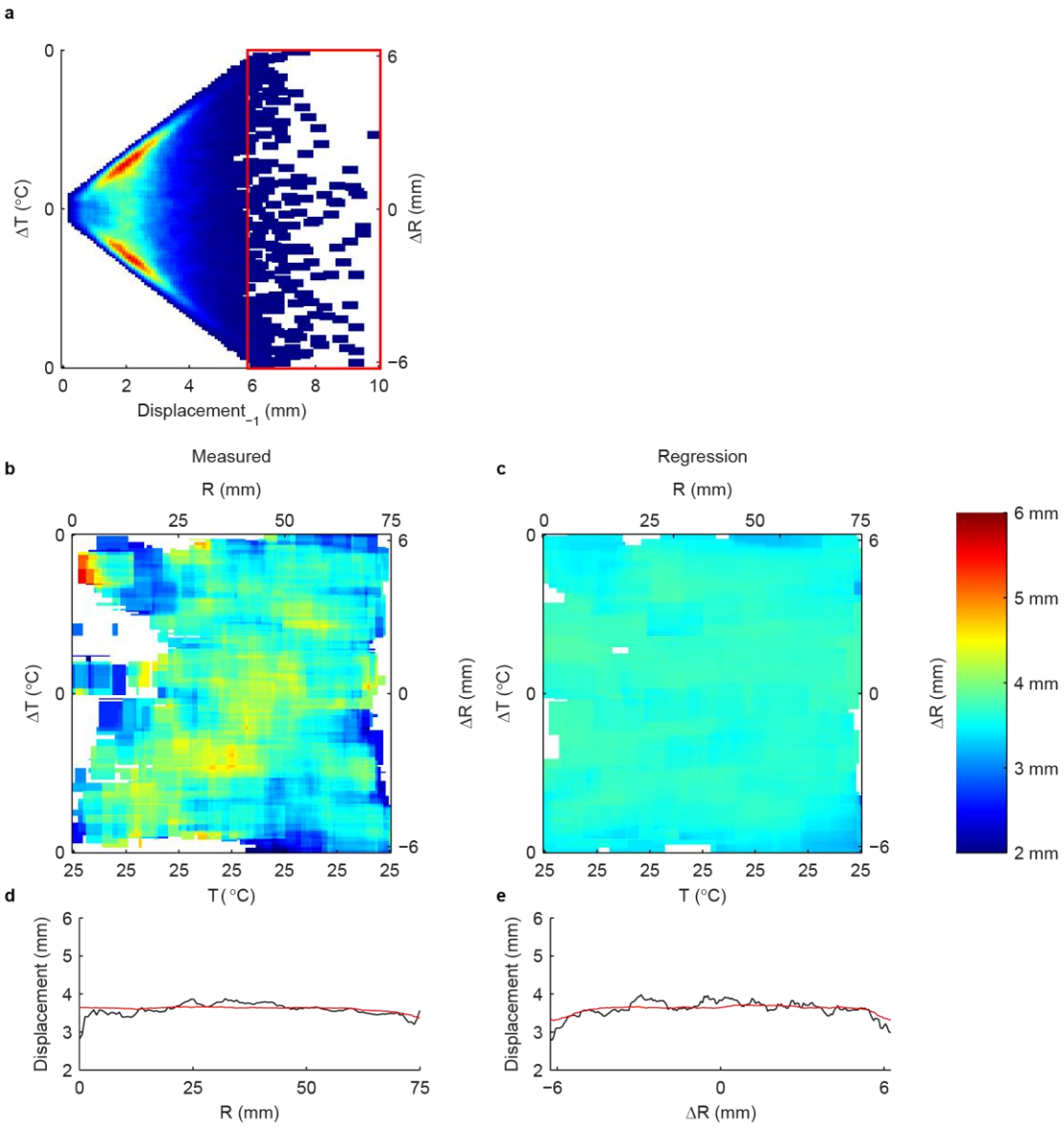

Figure 20 | Relationship between *R*, *ΔR*, and displacement in the baseline condition for a subset of the data where predictors are uncorrelated. a, Joint probability density map of previous displacement and Δ*R*. In the subset of the data indicated in the red box, these variables are uncorrelated. The remainder of the figure analyzes this subset of the data. **b,** Conditional expected value of displacement given *R* and Δ*R*. **c,** Predicted value of displacement using linear regression model. **e-f,** Estimated displacement by KDE (black line) and regression (red line) as a function of *R* (**c**) and Δ*R* (**d**).

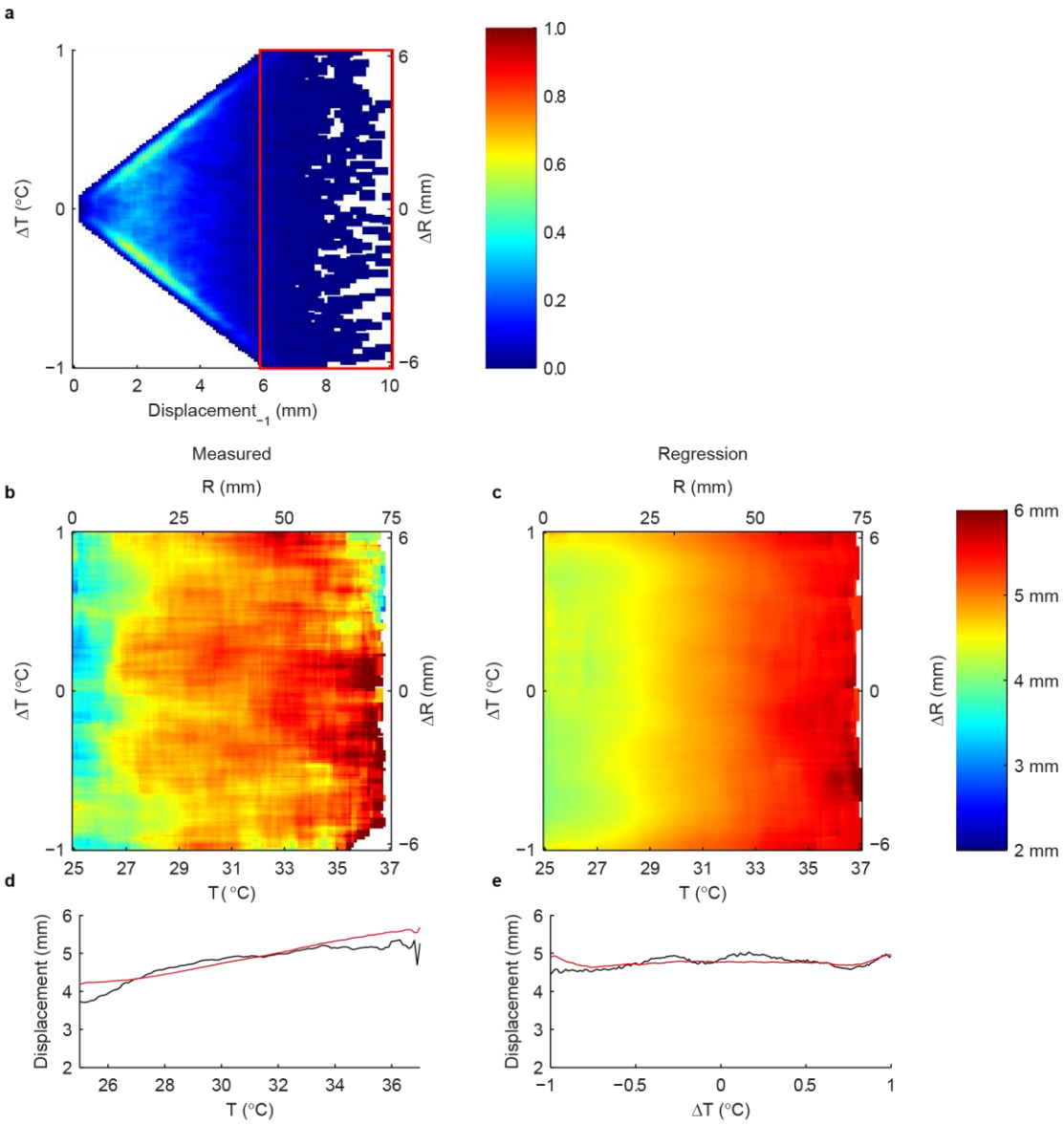

Figure 21 | Relationship between *T*, *ΔT*, and displacement in the gradient condition for a subset of the data where predictors are uncorrelated. a, Joint probability density map of previous displacement and Δ*T*. In the subset of the data indicated in the red box, these variables are uncorrelated. The remainder of the figure analyzes this subset of the data. **b,** Conditional expected value of displacement given *T* and Δ*T*. **c,** Predicted value of displacement using linear regression model. **e-f,** Estimated displacement by KDE (black line) and regression (red line) as a function of *T* (**c**) and Δ*T* (**d**).

4.3 DWELL TIME

We used KDE and linear regression to measure the relationship between T, ΔT, $displacement_{-1}$, and dwell time (R, ΔR in the baseline condition). We find that in the baseline condition, dwell time is related to previous displacement but not affected by R or ΔR (**Fig. 22** and **Table 4**). By contrast, we find that during the gradient condition dwell time decreases as a function of T and is not largely affected by ΔT (**Fig. 23** and **Table 5**).

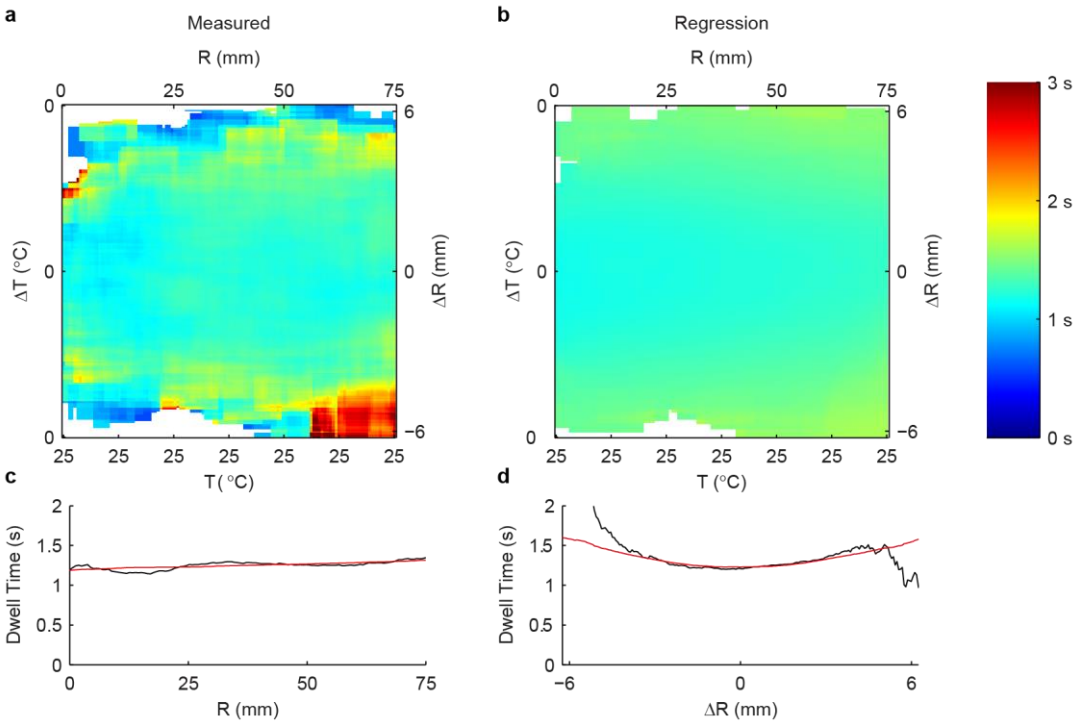

Figure 22 | Relationship between *R*, *ΔR*, and dwell time in the baseline condition. a, Conditional expected value of dwell time given R and ΔR. **b,** Predicted value of dwell time using the linear regression model in **Table 4**. **c-d,** Estimated dwell time by KDE (black line) and regression (red line) as a function of R (**c**) and ΔR (**d**).

Table 4 | Linear regression model for dwell time in baseline condition.

Dwell time ~ 1 + *R* + *Displacement*$_{-1}$

	Estimated Coefficient	p-value
Intercept	1.004 ± 0.028	$< 1.0 \cdot 10^{-20}$
R	0.009 ± 0.003	$7.4 \cdot 10^{-4}$
Displacement$_{-1}$	0.074 ± 0.007	$< 1.0 \cdot 10^{-20}$

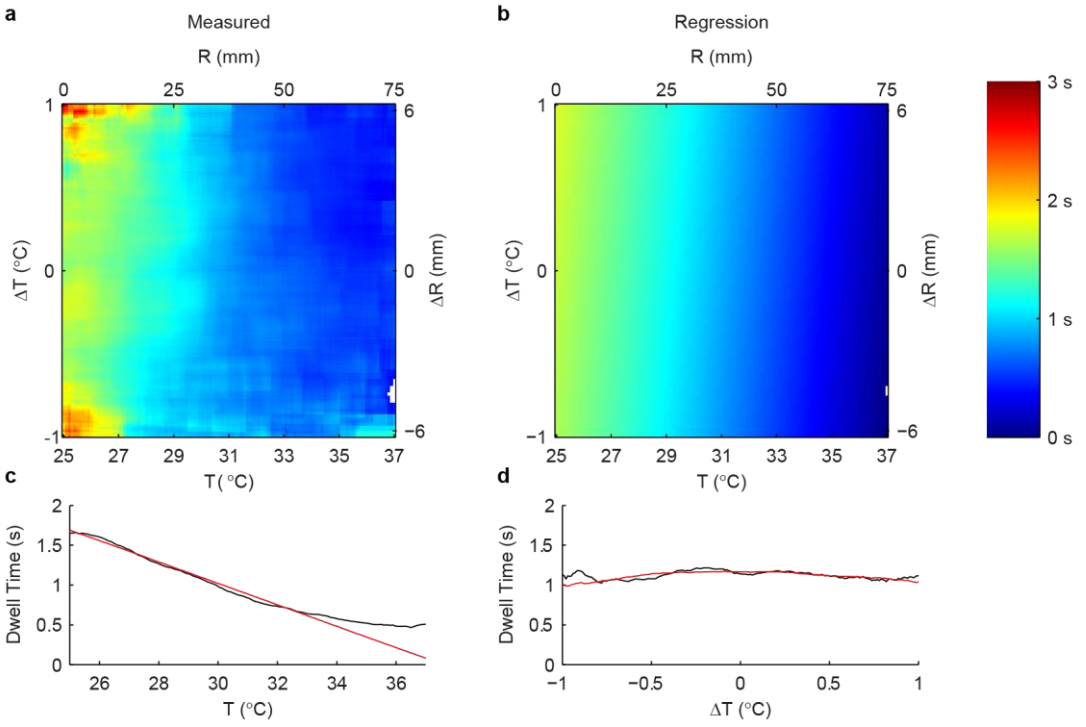

Figure 23 | Relationship between *T*, *ΔT*, and dwell time in the gradient condition. a, Conditional expected value of dwell time given *T* and Δ*T*. **b,** Predicted value of dwell time using the linear regression model in **Table 5**. **c-d,** Estimated dwell time by KDE (black line) and regression (red line) as a function of *T* (**c**) and Δ*T* (**d**).

Table 5 | Linear regression model for dwell time in the gradient condition.

Dwell time ~ 1 + *T* + ΔT

	Estimated Coefficient	p-value
Intercept	1.697 ± 0.014	$< 1.0 \cdot 10^{-20}$
T	-0.136 ± 0.003	$< 1.0 \cdot 10^{-20}$
ΔT	0.072 ± 0.019	$1.6 \cdot 10^{-4}$

4.4 Turn Magnitude

We used KDE and linear regression to measure the relationship between T, ΔT, $displacement_{-1}$, and turn magnitude (R, ΔR in the baseline condition). We find that in the baseline condition, average turn magnitude is essentially flat at around 25° (**Fig. 24** and **Table 6**). Unlike displacement and dwell time, $displacement_{-1}$ is not a highly significant predictor of current turn magnitude. During the gradient condition, we find that turn magnitude increases as a function of T and also ΔT, and is modulated to a lesser extent by previous displacement (**Fig. 25** and **Table 7**).

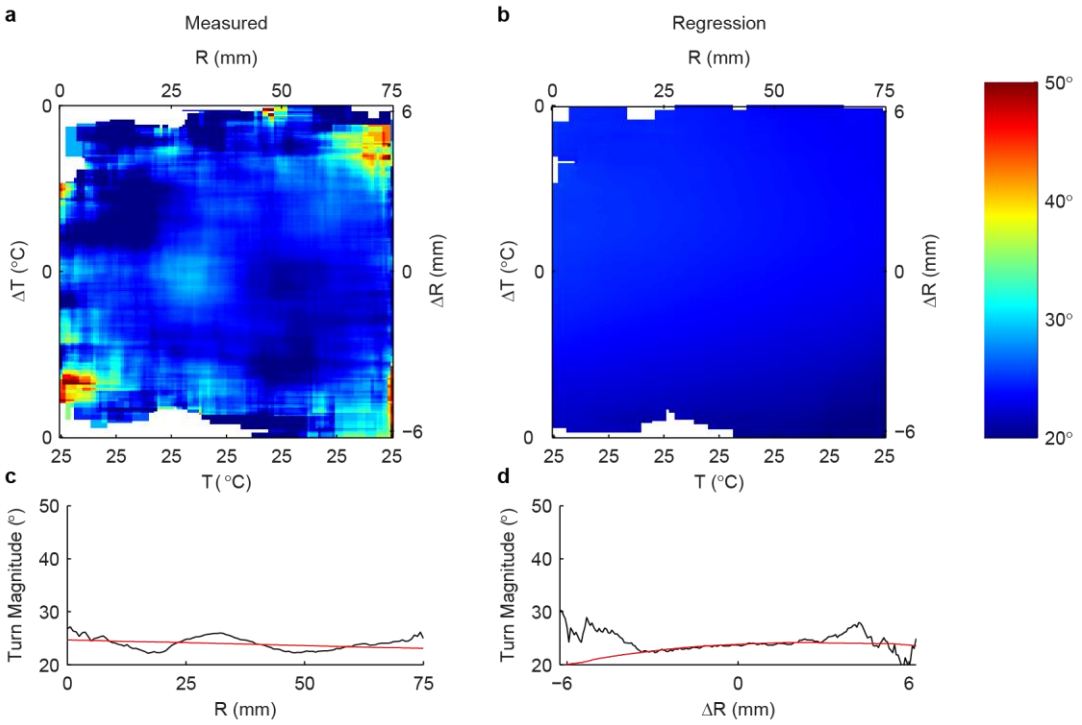

Figure 24 | Relationship between *R*, *ΔR*, and turn magnitude in the baseline condition. a, Conditional expected value of turn magnitude given R and ΔR. **b,** Predicted value of turn magnitude using the linear regression model in **Table 6**. **c-d,** Estimated turn magnitude by KDE (black line) and regression (red line) as a function of R (**c**) and ΔR (**d**).

Table 6 | Linear regression model for turn magnitude in the baseline condition.

Turn magnitude ~ 1 + *R* + Δ*R* + *Displacement*$_{-1}$

	Estimated Coefficient	p-value
Intercept	25.847 ± 0.020	$< 1.0 \cdot 10^{-20}$
R	-0.147 ± 0.073	$4.5 \cdot 10^{-2}$
Δ*R*	1.708 ± 0.607	$4.9 \cdot 10^{-3}$
Displacement$_{-1}$	-0.415 ± 0.175	$1.8 \cdot 10^{-2}$

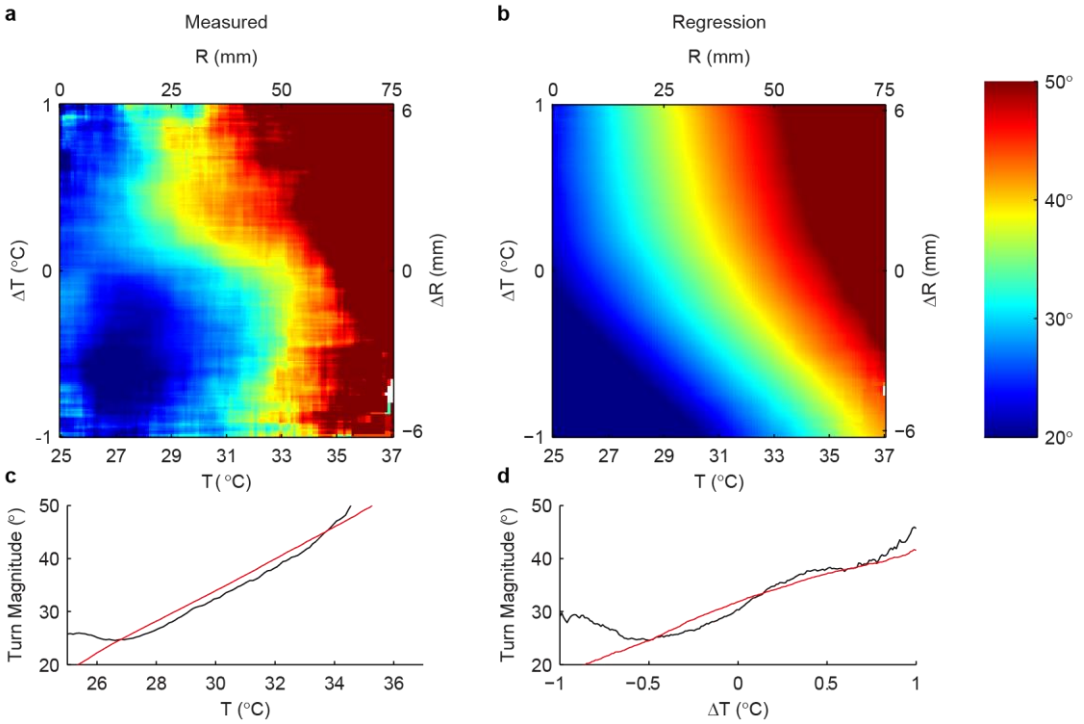

Figure 25 | Relationship between *T*, *ΔT*, and turn magnitude in the gradient condition. a, Conditional expected value of turn magnitude given *T* and Δ*T*. **b,** Predicted value of turn magnitude using the linear regression model in **Table 7**. **c-d,** Estimated turn magnitude by KDE (black line) and regression (red line) as a function of *T* (**c**) and Δ*T* (**d**).

Table 7 | Linear regression model for turn magnitude in the gradient condition.

Turn magnitude ~ 1 + T + ΔT + $Displacement_{-1}$

	Estimated Coefficient	p-value
Intercept	23.578 ± 0.463	$< 1.0 \cdot 10^{-20}$
T	3.045 ± 0.071	$<1.0 \cdot 10^{-20}$
ΔT	10.574 ± 0.454	$<1.0 \cdot 10^{-20}$
$Displacement_{-1}$	-1.390 ± 0.116	$<1.0 \cdot 10^{-20}$

4.5 Turn Direction

In previous studies of navigation in zebrafish, it has generally been assumed that turn direction is randomly selected and not affected by temporal stimuli. Surprisingly, we observed prolonged periods on the order of minutes where a particular turn direction was favored after experiencing a positive ΔT (**Fig. 26**). To quantify this effect, we defined a state variable that we refer to as the turn state, which takes a value of +1 or -1 depending on whether left or right turns are more strongly associated with movements following $\Delta T > 0$. We use a window size of 200 preceding movements, which corresponds to ~5min.

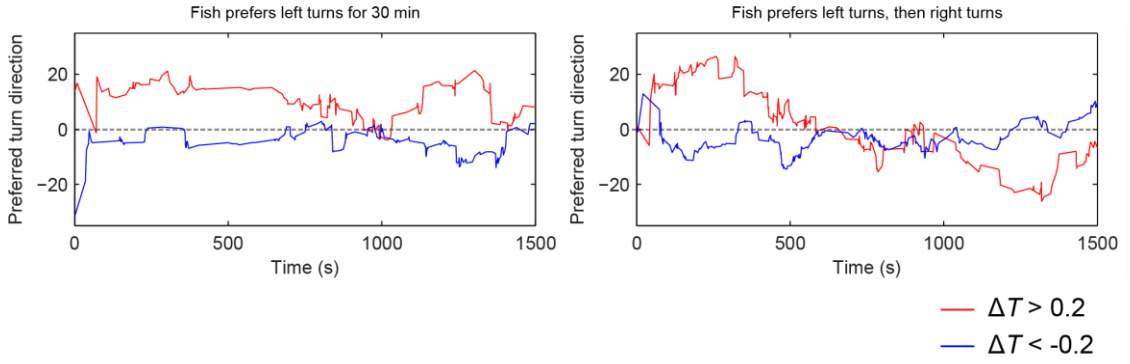

Figure 26 | Examples of two 7 dpf larval zebrafish showing prolonged preference for a particular turn direction in response to positive Δ*T*.

In any given thermosensory context (T, ΔT), we can measure how frequently the next move is in the direction specified by the turn state, and how frequently it is opposite to the turn state. We refer to

this quantity as the turn bias in a given context and report this quantity as a scaled value from -1 to +1, where -1 would mean that all turns oppose the turn state and +1 would mean that all turns are in the direction of the turn state. In the next section, we will show that knowing the turn state of a given fish and whether the preceding movement had a positive or negative Δ*T*, we can predict the direction that the fish is likely to turn in response to this preceding Δ*T*. Thus, the relevant axis for thinking about turn direction in our assay appears to be a thermosensory valence axis, in which one direction is associated with positive changes in temperature and the other direction is associated with negative changes in temperature.

We used KDE and linear regression to measure the relationship between *T*, Δ*T*, $displacement_{-1,}$ and turn bias (*R*, Δ*R* in the baseline condition). We find that in the baseline condition, average turn bias is essentially flat at 0.024 (**Fig. 27** and **Table 8**), and regression found no predictors for any spontaneous turn bias. In contrast, in the gradient condition, we find that turn bias is most strongly and significantly modulated by Δ*T* (**Fig. 28** and **Table 9**).

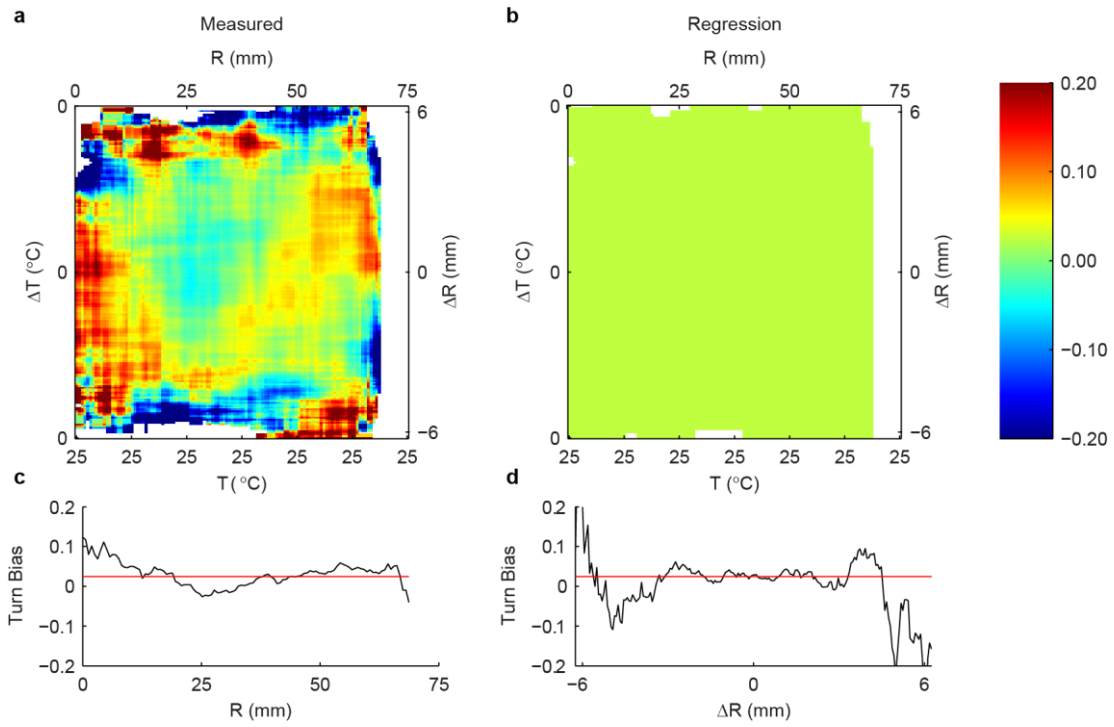

Figure 27 | Relationship between *R*, *ΔR*, and turn bias in the baseline condition. a, Conditional expected value of turn bias given *R* and Δ*R*. **b,** Predicted value of turn bias using the linear regression model in **Table 8**. **c-d,** Estimated turn bias by KDE (black line) and regression (red line) as a function of *R* (**c**) and Δ*R* (**d**).

Table 8 | Linear regression model for turn bias in the baseline condition.

Turn direction bias ~ 1

	Estimated Coefficient	p-value
Intercept	0.024 ± 0.008	$2.9 \cdot 10^{-3}$

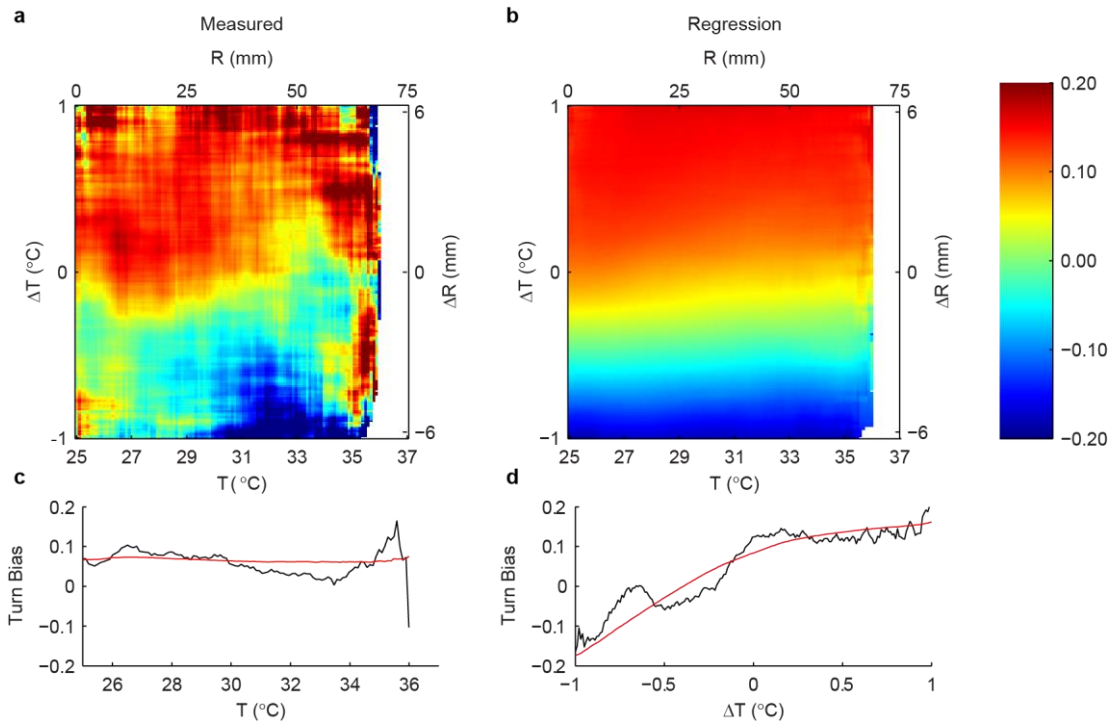

Figure 28 | Relationship between *T*, *ΔT*, and turn bias in the gradient condition. a, Conditional expected value of turn bias given *T* and Δ*T*. **b,** Predicted value of turn bias using the linear regression model in **Table 9**. **c-d,** Estimated turn bias by KDE (black line) and regression (red line) as a function of *T* (**c**) and Δ*T* (**d**).

Table 9 | Linear regression model for turn bias in the gradient condition.

Turn direction bias ~ 1 + Δ*T* + *Displacement*$_{-1}$

	Estimated Coefficient	p-value
Intercept	0.144 ± 0.017	2.0e-17
Δ*T*	0.167 ± 0.018	<1.0e-20
Displacement$_{-1}$	-0.023 ± 0.004	2.9e-7

5 SUMMARY OF THERMOSENSORY RELATIONSHIPS

We used KDE and regression to measure the relationship between absolute temperature, recent changes in temperature, and each of the components of a movement event. We find that dwell time is reduced as a function of *T*. In other words, larvae move more rapidly at high temperatures regardless of whether the temperature has just increased or decreased. Displacement increases as a function of *T*.

This means that larvae travel longer distances per movement at high temperatures regardless of whether the temperature has just increased or decreased. Unlike dwell time and displacement, turn magnitude is positively modulated by both T and ΔT, meaning that larvae turn more strongly at high temperatures and after movements heading up the gradient. Finally, turn bias is predominantly modulated by ΔT. Thus, when larvae move up the gradient, they tend to bias their turns so that they consistently turn toward the direction currently specified by their turn state. Once they start moving down the gradient, they cease to strongly bias their turns in the preferred turn direction. After relatively large temperature drops, larvae can even bias their turns in away from the direction currently specified by their turn state.

Taken together, the relationships between these motor elements and thermosensory experience represent a possible strategy for thermal navigation. As larvae swim toward higher temperatures (i.e. increase in T and ΔT), they move farther, make larger turns, and are more likely to turn in their preferred direction. When animals swim down the gradient, they reorient less and can even show a modest bias against the preferred direction. These relationships allow fish to abort trajectories heading up the gradient while preferentially committing to favorable headings leading down the gradient.

During the gradient condition, we observe an overall positive correlation in turn direction but an anti-correlation in turn direction after previous rising and falling temperatures. These correlations across individual movement events can potentially contribute to successful navigation. Consider the case where all turn directions were positively correlated regardless of temperature. After an animal has made multiple turns in its preferred direction to return to a favorable heading, if the turn direction bias remained unchanged, then there would be a high chance that the animal will loop back toward the unfavorable heading after further turns. In reality, the turn direction preference switches as the heading becomes increasing favorable, which may act as a braking mechanism to prevent the animal from

looping back toward unfavorable headings. Our results raise an interesting hypothesis: differential expression of turn direction bias as a function of thermosensory experience may represent a key component of the strategy that zebrafish use for thermal navigation.

It is important to note that zebrafish predominantly navigate the thermal gradient using routine turns. Our high speed imaging system allows us to detect escape movements that have been extensively described in the zebrafish literature in response to sudden or noxious stimuli. Aside from an occasional escape behavior upon first encountering the noxious extremes of the chamber, the remainder of the thermal navigation behavior consists of routine turns. The importance of this observation is that zebrafish navigate the thermal gradient by turning frequently but relatively gently, so that individual reorientations are generally insufficient to convert unfavorable headings to favorable ones. Under these conditions, we propose that maintaining a preferred direction is essential to ensuring that a sequence of turns will cumulatively reorient the animal toward a favorable heading, instead of meandering about a mean heading change of 0°. We will evaluate the contribution of this movement component to thermal restriction when we simulate thermal navigation in the next chapter.

6 RESPONSE TO THERMOSENSORY EXPERIENCE IN THE ABSENCE OF SPATIAL NAVIGATION

Our analysis of locomotion during thermal navigation suggests that the strategy by which zebrafish navigate the gradient is by modulating their movement rate, displacement, turn magnitude, and turn direction as a function of thermosensory experience. To resolve whether the sensorimotor correlations that we observed in the gradient were specific to spatial navigation or are generally representative of how zebrafish respond to temperature, we assayed locomotion in response to spatially uniform time-varying thermal waveforms. This assay is crucially different from the gradient assay because the thermal stimulus is presented in open loop, meaning that the stimulus is presented

irrespective of the animal's behavioral response. This allows us to eliminate any potential operant component of the navigation behavior and determine which locomotor relationships are intrinsic to how zebrafish respond to thermal experience.

We chose to focus on delivering sinusoidal thermal stimuli at three different baseline temperatures in order to vary both absolute and relative temperature. We superimposed a 2 °C peak-to-peak sinusoidal oscillation on top of baseline temperatures of 25 °C, 30 °C, and then 35 °C for 12 min each while monitoring the behavioral response. These baseline temperatures were chosen to span relevant temperatures in the thermal gradient. The chosen thermal stimulus allows us to measure how each component of movement varies as a function of absolute and relative temperature in an open loop setting.

We find that the thermal waveform chamber generally recapitulates the relationships between locomotor elements and temperature that we observed in the radial gradient. Turn magnitude is modulated by both absolute temperature and relative temperature (**Fig. 29, Fig. 30**). Turn direction bias showed a relationship to relative temperature (**Fig. 29, Fig. 31**).

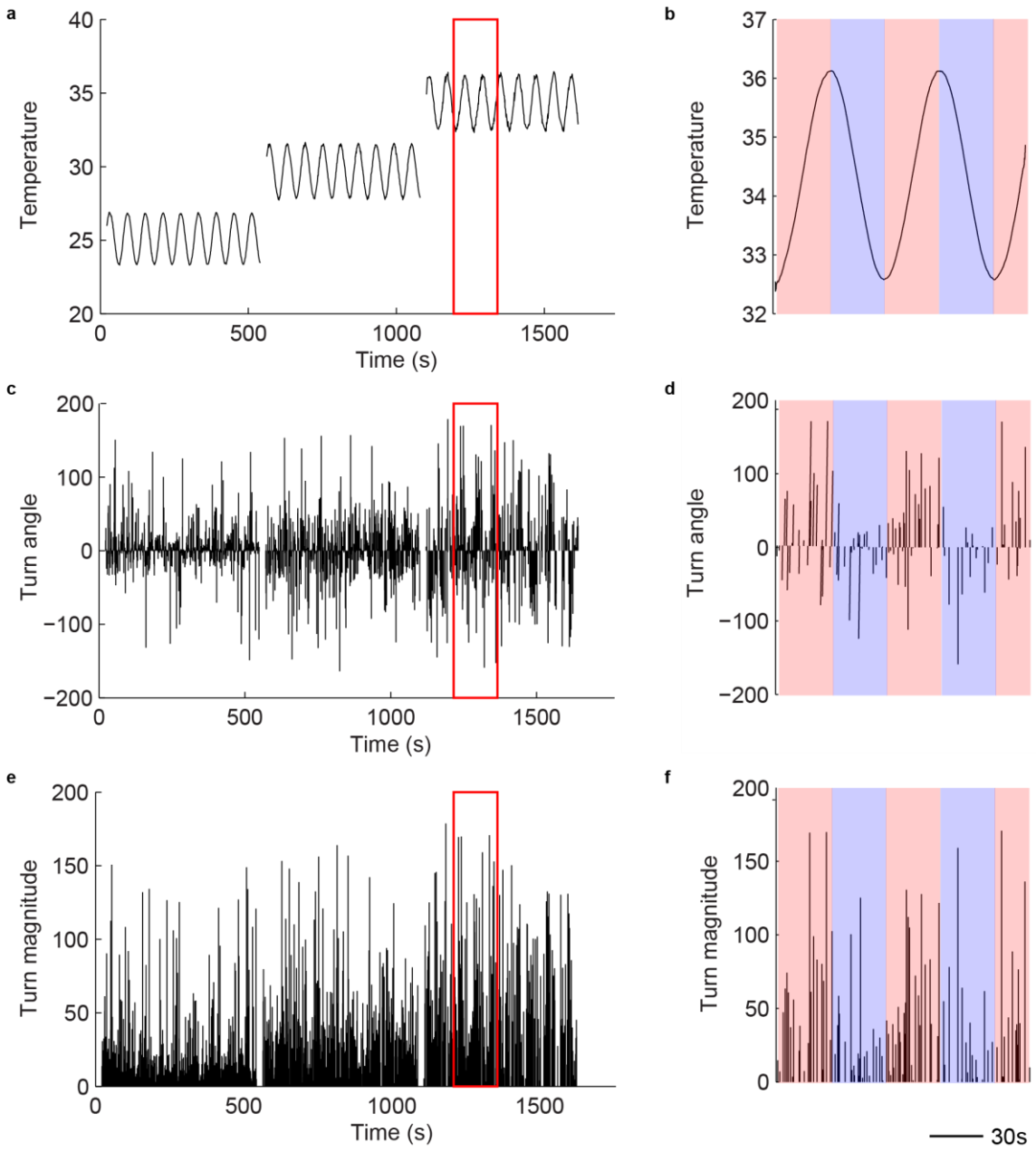

Figure 29 | Example of a 7 dpf zebrafish responding to sinusoidal thermal stimuli. a, Sinusoidal thermal stimulus was presented at three baseline temperatures with a 2 °C peak to peak amplitude oscillation. **b,** Responses were analyzed relative to the phase of the stimulus. **c,** Summary of turn angles of movement events throughout the stimulus. Red box marks the extents of the zoomed region. **d,** Zoom of turn angles occurring during two cycles of the thermal stimulus at a high baseline temperature. During the selected time period, the animal preferred positive (right) turns during rising temperature, which would correspond to a turn state of +1. **e,** Summary of turn magnitudes throughout the thermal stimulus. Turn magnitude tends to increase as a function of the absolute temperature. Red box marks the extents of the zoomed region. **f,** Zoom of turn magnitudes during two cycles of the thermal stimulus at a high baseline temperature. Turn magnitudes are higher during the rising phase than the falling phase.

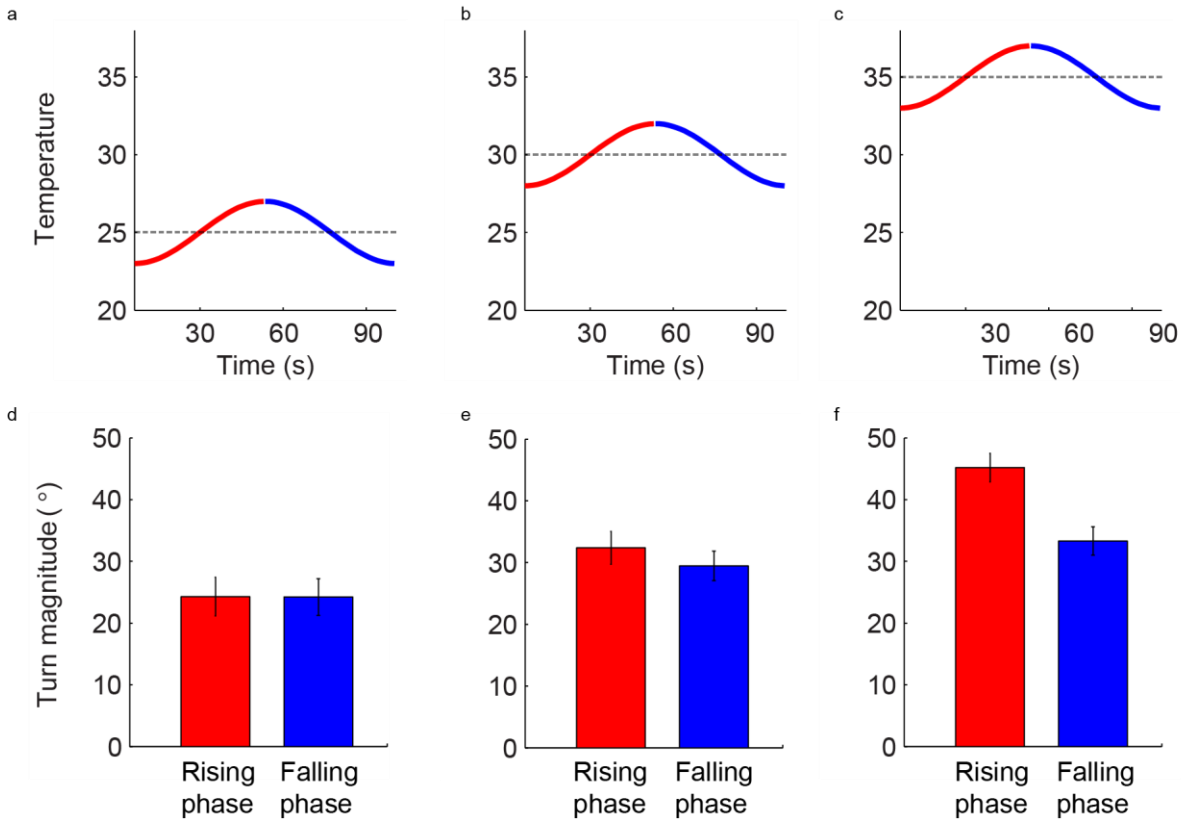

Figure 30 | Population-averaged turn magnitude as a function of baseline temperature and rising or falling phase. Turn magnitudes increase as the baseline is increased from 25 °C (**a,d**) to 30 °C (**b,e**) and 35 °C (**c,f**). At 35 °C, average turn magnitude during the rising phase significantly exceeds the falling phase.

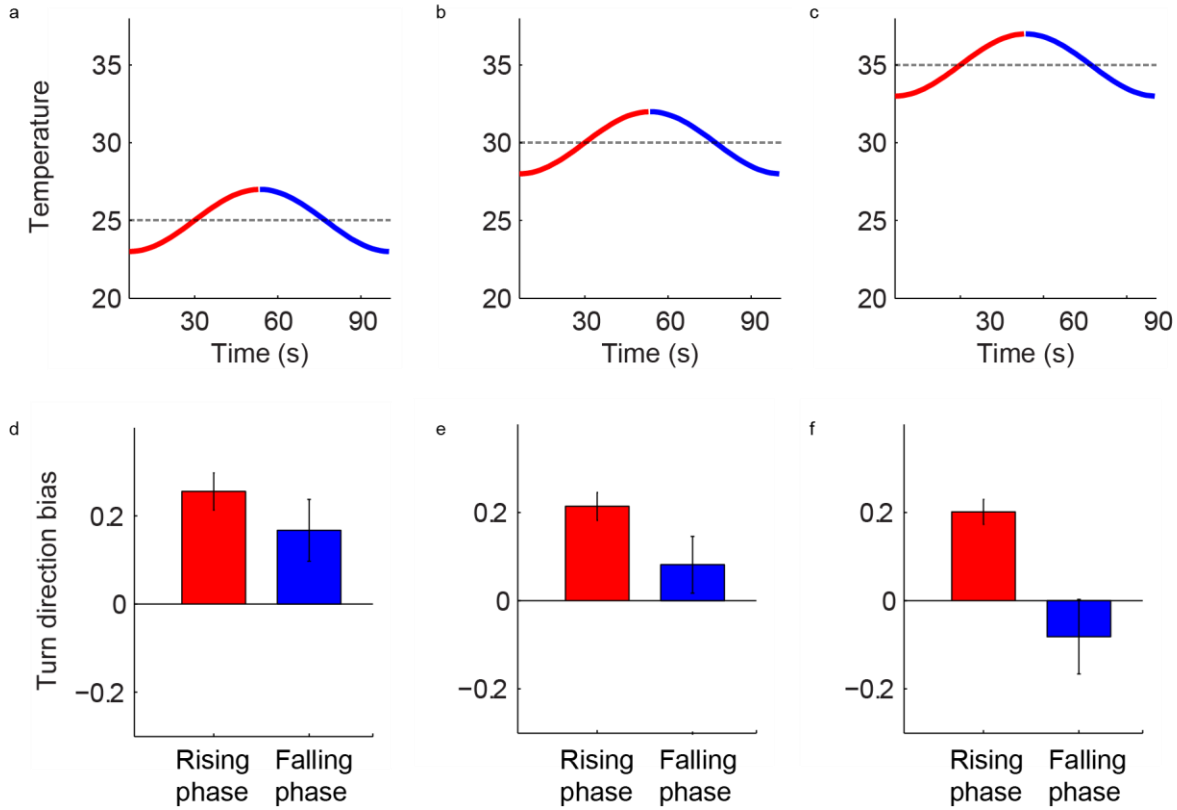

Figure 31 | Population-averaged turn bias as a function of baseline temperature and rising or falling phase. Turn bias is elevated at all baseline temperatures during rising phase, but decreases and becomes negative during the falling phase as the baseline temperature increases.

We also analyzed the preferred turn direction in the sine wave experiment. Since preferences in turn direction are not absolutely stable across the time course of the experiment, we adopted a local definition of the preferred turn direction. Specifically, we averaged the turn direction of two turns prior and two turns following a given movement and defined the preferred turn direction at the time of the movement as the sign of this average. We avoided incorporating the turn angle of the turn in question to avoid circularity and ensure that any observed correlation was not an artifact of our definition.

We find that turns occurring during the rising phase of the sine wave correlate with the preferred turn direction. This effect is strongest when the sine wave occurs around 35 °C but is apparent at all temperatures tested. In contrast, we find that turns during the falling phase of the sine wave show

either random direction or else weak anticorrelation to the preferred turn direction during heating. The behavioral results in the thermal waveform chamber support the interpretation that larvae possess an intrinsic strategy in response to thermosensory experience that is effective in navigating the thermal gradient.

We also investigated the stability of the preferred turn direction in both the radial gradient and thermal waveform assays. We find that a turn preference in a given direction is typically stable for 5-10 min. In the radial gradient, we note that some animals can maintain the same preferred turn direction for the entire 30 min of the behavior (**Fig. 25**). This preference appears to be more stable than the turn direction preference that we measure in the thermal waveform chamber. One possibility is that the sensory feedback received while navigating the thermal gradient stabilizes a spontaneous turn direction preference. This is consistent with our other work on operant learning in larval zebrafish. Briefly, a tethered larval zebrafish presented with a stable response-outcome contingency (e.g. left turns abolish noxious heat) can be trained to stably prefer the rewarded turn direction for at least 1 hour. We hypothesize that in the thermal gradient, some animals experience a stable response-outcome contingency because their preferred turn direction leads them to circle the gradient in a consistent direction (i.e. clockwise or counterclockwise). As long as the animal traverses the gradient in the same clockwise or counterclockwise direction, noxious heat consistently lies on the same side of the animal's heading, and the same turn direction will consistently lead to lower temperature outcomes. Nevertheless, the majority of fish do not "lock in" a preferred direction for the entire duration of the navigation experiment, presumably because random heading reversals place the gradient on either side of their heading and break up the coherence of any one response-outcome relationship.

7 CONCLUSION AND DISCUSSION

Our analysis of thermal navigation in larval zebrafish reveals that zebrafish can modulate many locomotor elements in response to absolute and relative temperature experience in order to enrich for favorable headings down the gradient. We were able to broadly recapitulate the observed relationships in an open loop setting in which the presentation of thermal steps and sine waves was uncoupled from spatial navigation. Finally, we observed that zebrafish can modulate the expression of a preferred turn direction to reduce the number of turns required to explore alternative headings when the present heading is unfavorable.

Compared to the established invertebrate models of thermotaxis, zebrafish navigate somewhat differently. Negative thermotaxis in *C. elegans* has been described as a biased random walk, in which unfavorable runs of forward movement leading to higher temperatures are shortened by an elevated rate of reorientation events, called pirouettes, which randomize the heading of the animal. Thus, *C. elegans* can extend the time spent following favorable headings, but the manner in which it selects a favorable heading is by random trial and error. Zebrafish locomotion is somewhat incompatible with this mechanism of thermotaxis. Unlike the continuous forward runs in *C. elegans*, zebrafish move in discrete bouts. Furthermore, zebrafish movement sequences do not show a clear cut distinction between forward runs and turns. All zebrafish movements typically result in some degree of forward displacement and reorientation.

Compared to *Drosophila* thermotaxis, zebrafish show both similarities and differences. Both Drosophila larvae and zebrafish larvae bias the magnitude of their turns in response to rising temperature. However, the strategy for selecting the turn direction is clearly distinct between *Drosophila* and zebrafish. During negative thermotaxis, Drosophila larvae perform one or more test head sweeps to sample the local spatial variation in temperature before each reorientation, and then

preferentially commit to a head sweep that led to a reduction in temperature. Zebrafish locomotion is fundamentally different. Zebrafish routinely commit to displacements equal to their body length and reorientations of 30-60° every second. Without a dedicated sampling phase before each movement, zebrafish must have a heuristic for optimizing turn direction on the go. We have shown that zebrafish solve this problem in a novel way, by consistently favoring a preferred turn direction in response to rising temperature and then suppressing the expression of this preference when temperature is flat or falling. We believe this strategy represents a viable navigation strategy for animals that do not test the consequences of every potential action before they commit them. We have collected anecdotal evidence that when deprived of other sensory cues, humans may use a similar strategy.

8 METHODS

High speed infrared imaging of freely behaving larval zebrafish

We monitored locomotion in the radial gradient at 500 frames per second using a 1.3 megapixel (MP) high speed CMOS camera (Mikrotron) and a Cameralink framegrabber (National Instruments) while providing overhead infrared illumination with an octagonal array of 950 nm LEDs (OSRAM). We monitored locomotion in the thermal waveform chamber at 240 frames per second with a 1.3 MP CMOS USB3 camera (Point Grey) operating in region of interest (ROI) mode with software-triggered panning to keep the fish in the ROI.

Fish tracking

Our software tracks the fish by maintaining a background model of the behavioral chamber and subtracting the background from every acquired camera frame. We then detect the eyes of the fish in random order by finding the strongest background subtracted signal, removing it from the image, and then finding the next strongest signal. Once the location of both eyes is determined, we can use simple

geometry to obtain a line that runs parallel to the major body axis of the fish. We determine which way the fish is pointing along this line by performing a local line search in both directions starting from the head point, and then compare the averaged background subtracted intensity in each direction to determine which way points in front of the fish. We track the position of 8-10 segments along the tail by sequentially walking from head to tail while intersecting a perpendicular line with the tail and performing a line search to maximize a symmetry metric.

Decoding of movements

We calculate the velocity of the animal by applying a Gaussian differentiation filter to the coordinates of the fish's head. We threshold the velocity and define a new movement event each time the velocity crosses this threshold from below and then eventually becomes stationary again. We extract the dwell time by calculating the time elapsed since the last move. We calculate the displacement by calculating the distance from the last position before the move where the fish had zero velocity to the first position after the move that the fish had zero velocity. We calculate the turn magnitude as the absolute value of the change in heading angle before and after a move. To define the preferred turn direction at the time of a movement event, we filter the neighboring turns before and after the movement event so that we only consider those movements that followed a rising temperature change of $\Delta T > 0.2$. We define the locally preferred turn direction as the sign of the average turn angle obtained from the previous two filtered moves along with the next two filtered moves.

4. Behavioral simulations of thermal navigation strategies

1 ABSTRACT

Our quantitative measurements of zebrafish locomotion during thermal navigation behavior reveal that thermosensory experience modulates multiple locomotor elements, including dwell time, displacement, turn magnitude, and turn direction bias. We next turned to behavioral simulations to determine whether a comprehensive model incorporating thermosensory modulation of all of these motor elements could recapitulate the thermal restriction that we observe in the radial gradient. Behavioral simulations are also a powerful way to assess the importance of individual sensorimotor relationships, since we can arbitrarily add or remove individual components of the proposed strategy and evaluate the consequence to navigation performance. We find that a comprehensive model that incorporates thermosensory modulation of all four locomotor elements fully recapitulates the observed thermal restriction of larval zebrafish. The most important motor element is turn magnitude, followed closely by turn direction bias. Nevertheless, our behavioral simulations reveal that each of the measured locomotor elements enhances thermal restriction. Our results demonstrate that larval zebrafish use thermosensory information to modulate all aspects of their locomotion to optimize navigation.

2 INTRODUCTION

Our quantitative measurements of zebrafish locomotion during thermal navigation behavior reveal that thermosensory experience modulates multiple locomotor elements, including dwell time, displacement, turn magnitude, and turn direction bias. There are a number of important questions that we can ask about these relationships. Firstly, we need to determine whether a comprehensive model incorporating all of these sensorimotor relationships is sufficient to recapitulate the thermal restriction

that we observe in the radial gradient assay. This allows us to conclude whether we have already identified and correctly extracted the components of the navigation strategy, or we should still be looking for further components to fully explain the behavior. Behavioral simulations are also a powerful way to assess the importance of individual sensorimotor relationships, since we can arbitrarily add or remove individual components of the proposed strategy and evaluate the consequence to navigation performance.

In this chapter, we will present our approach to simulating the stochastic process of thermal navigation in larval zebrafish. We will begin with a "blank slate" model that captures the distribution of each locomotor element as zebrafish navigate the gradient but does not vary based on thermosensory experience. This model would be expected to show uniform coverage of the simulated chamber because moves are stochastically selected without regard for temperature. We will then consider the effect of incorporating thermosensory modulation into just one locomotor element. After adding the motor element that most improves thermal restriction, we will sequentially repeat this process until dwell time, displacement, turn magnitude, and turn direction bias are all incorporated into the model. We can then determine whether we need to find and extract additional relationships between thermosensory experience and locomotion, or whether our model can already recapitulate the behavior.

3 SIMULATING THERMAL NAVIGATION

We simulate zebrafish locomotion using standard Monte Carlo methods. At each T and ΔT, we estimate the probability distribution for each of the four locomotor elements -- dwell time, displacement, turn magnitude, and turn direction bias. Simply using the mean values for each locomotor element at every pair of T and ΔT would give us a simple deterministic model, but would not take in account the variance in the distribution of each motor element. By using the probability distribution for

each locomotor element at every pair of *T* and *ΔT*, we were able to incorporate naturally occurring behavioral stochasticity into our model.

To establish a baseline for the subsequent simulations, we generated simulated trajectories in the radial gradient using overall probability distributions of all four locomotor elements (**Fig. 31a**) across all *T* and *ΔT*. These distributions are not conditional on temperature in the baseline model. For each locomotor element, we sample from the same overall distribution regardless of *T* and *ΔT.* As expected, these trajectories cover the chamber area uniformly due to the lack of utilization of thermosensory information in any of the locomotor elements (**Fig. 31b**).

4 MODULATION OF TURN MAGNITUDE AND TURN DIRECTION BIAS ARE ESSENTIAL COMPONENTS OF THE LARVAL NAVIGATION STRATEGY

We attempted to incrementally build a complete model of thermal navigation by adding the motor element that improved thermal restriction the most. We found that introducing thermosensory modulation to the turn magnitude had by far the most favorable effect on thermal restriction (**Fig. 31c-d**). In fact, out of the four locomotor elements that we considered, turn magnitude was the only element that had a clear impact on thermal restriction on its own. This component of the zebrafish navigation strategy is similar to Drosophila, where it has already been established that biasing toward larger turns in response to unfavorable headings is an effective strategy for rapidly reacquiring favorable headings. Nevertheless, simulating this strategy alone leaves much of the observed thermal restriction unexplained. Observed thermal restriction peaks at 27.5°C, while the simulated thermal restriction using only turn magnitude peaks at 31.3°C.

After adding thermosensory modulation of turn magnitude to the model, we tested the incremental improvement in thermal restriction of adding sensorimotor relationships for dwell time, displacement, or turn direction bias. We now found that all of these motor elements provided some

degree of behavioral improvement, indicating that although these elements do not inherently confer navigation ability, they are capable of enhancing navigation by acting in concert with other motor elements. We found that conditioning the turn direction bias on thermosensory experience led to the greatest improvement in thermal restriction (**Fig. 31e-f**). The combination of turn magnitude and turn direction bias can already largely recapitulate the thermal restriction we observe in the thermal navigation behavior, and hence represent the core of the behavioral strategy. It is easy to see why these two motor strategies are particularly effective in navigation since both are closely involved in the selection of new headings. These strategies are especially important because zebrafish lack a dedicated sampling phase, such as head sweeps in Drosophila larvae and weathervaning in *C. elegans* chemotaxis. We argue that since zebrafish cannot test their turns before they commit to them, and because their routine turns are typically too small to identify a new favorable heading in a single movement, there is a need for a mechanism that links turns together so that they can accumulate constructively to lead to favorable heading changes. As shown in **Fig. 27**, turn direction bias is sharply split across the ΔT axis, such that animals are quite likely to turn again in their preferred direction for as long as temperature is increasing. Importantly, this correlation is abolished or even becomes anticorrelated in response to falling temperature. This could effectively function as a braking mechanism to ensure that strings of unilateral turns are interrupted once temperature has improved, thus avoiding overshoot in the heading adjustment.

Combining both turn rate and turn direction bias reveals that these strategies complement one another and yield trajectories and thermal restriction relatively similar to what we observe in larval zebrafish. Nevertheless, some room for improvement in performance still remains when only incorporating modulated turn magnitude and modulated turn direction bias.

Figure 32 (continued on next page) | Simulations of thermal navigation strategies reveal that specific locomotor elements such as turn magnitude and turn direction bias contribute significantly to thermal restriction

a-b, A baseline simulation using the overall distribution of each locomotor element without modulation by absolute temperature (*T*) or relative changes in temperature (ΔT) yields broad trajectories (**a**) and no thermal restriction (**b**). **c-d,** Simulations that incorporate the modulation of turn magnitude by absolute and relative temperature significantly improve thermal restriction. **e-f,** Simulations that incorporate the modulation of turn magnitude and turn direction bias by absolute and relative temperature further improve thermal restriction by a significant margin. Incorporating thermal modulation of locomotor elements such as dwell time (**g-h**) and displacement (**i-j**) produces modest improvements in thermal restriction. Thermal restriction (**b,d,f,h,j**) is averaged over 1000 simulation runs. Shaded areas represent +/- 1 standard error of the mean.

Figure 32 continued

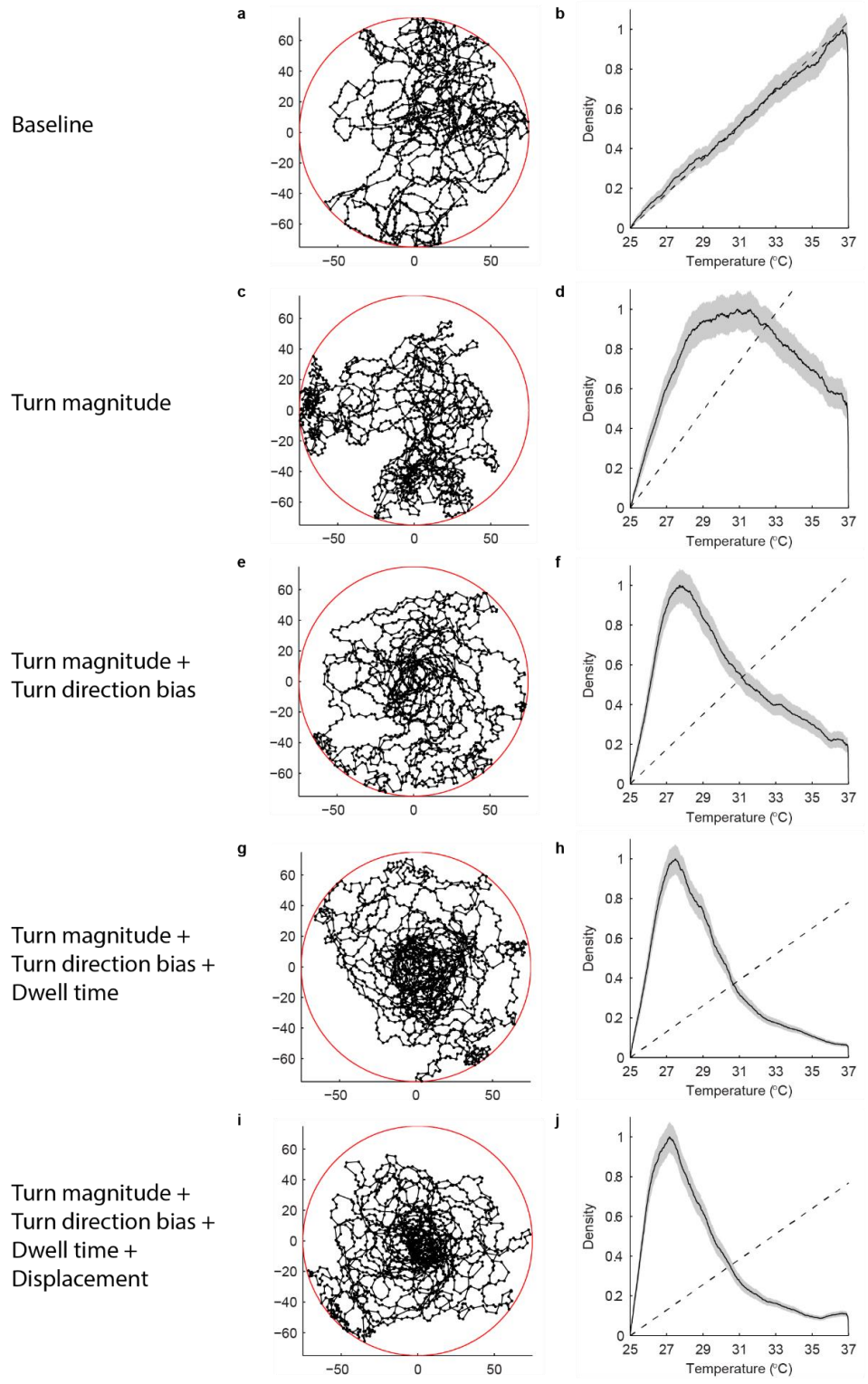

5 DWELL TIME AND DISPLACEMENT CONTRIBUTE TO THERMAL NAVIGATION

To continue developing our model, we tested whether making dwell time or displacement conditional on absolute and relative temperature would further improve the thermal restriction. We found that dwell time in particular was able to enhance thermal restriction (**Fig. 32g-h**). In contrast to the core components of the navigation strategy, dwell time has no direct effect on the selection of headings. Instead, it extends the time spent near the preferred temperatures in the center of the chamber and reduces the time it takes to find a better heading in the noxious parts of the chamber. Decreasing dwell time under unfavorable sensory conditions is an ideal addition to a core navigation strategy that can systematically identify favorable headings but requires multiple turns in order to accomplish it.

Finally, we allowed displacement to be modulated by thermal experience and found only a modest improvement in thermal restriction (**Fig. 32i-j**), perhaps because the thermal restriction of the simulation had already reached parity with real animals. We include the effect of thermal experience on displacement in our model but note that it contributes relatively less than the other locomotor elements.

6 CONCLUSION AND DISCUSSION

In this chapter, we stochastically simulated how zebrafish modulate locomotor elements in response to thermosensory experience in the radial gradient. We have shown that introducing thermosensory dependence to turn magnitude, turn direction bias, dwell time, and displacement provides incremental improvement to the ability of larvae to navigate the thermal gradient. Modulation of turn magnitude and turn direction bias form the core of the behavior. These two locomotor elements work tightly together to coordinate sequences of large turns in a preferred direction until a favorable heading is found. After experiencing a decrease in temperature, turn direction becomes either uncorrelated or anti-correlated to the preferred direction during rising temperatures. This switch in turn

direction bias prevents an overshoot in heading adjustment, while a coordinated decrease in turn magnitude promotes forward moving trajectories down the thermal gradient. Thermosensory experience also affects the dwell time between movements, allowing zebrafish to rapidly carry out avoidance trajectories consisting of many individual turns and extending the periods of time in which the animals occupy their preferred range of temperatures. Finally, the displacement per bout increases in response to unfavorable thermosensory experience, further potentiating the search for a favorable heading direction.

Our results raise the exciting possibility that these locomotor elements constitute a general navigation strategy in larval zebrafish beyond thermosensation. It would be interesting to test whether these locomotor elements have similar roles in mediating navigation behaviors in other modalities such as olfaction or vision. We have shown separable roles for the absolute and relative components of temperature in modulating locomotion, and it is possible that the same framework could be adapted to other stimuli as well.

By identifying specific sensorimotor mappings that are encoded by thermosensory circuitry along with their behavioral relevance, we also open up a promising entry point into the functional analysis of thermosensory circuitry by calcium imaging. We will discuss the implications of this work for calcium imaging in greater detail in the next chapter.

7 METHODS

We used standard Monte Carlo techniques to generate stochastic trajectories of freely swimming fish. The Monte Carlo framework itself is very simple. At the start of each run, we position a virtual animal at the center of a virtual radial thermal gradient. In each step of the run, we sample a new movement event by randomly selecting values for each motor element from some distribution. The key to obtaining realistic simulations is to correctly determine the correct probability distribution for each

locomotor element. The probability distributions that we used were based directly on our large dataset of more than 26,000 movements that we observed while animals navigated the thermal gradient. To calculate a given probability distribution, we discretized the set of possible values that a motor element could take. For example, we found that it was sufficient to discretize dwell time into increments of 0.2 s from 0.2 s to 10 s. We also discretized the possible values of T and ΔT, so that T ranged from 25 °C to 37 °C in increments of 0.1 °C and ΔT ranged from -1 °C to +1 °C in increments of 0.1 °C. Then, for every possible thermosensory scenario (e.g. T = 31.2 °C, and ΔT = +0.7 °C) and every possible outcome value (e.g. a dwell time of 3.2 s) we simply counted the number of times that we found a movement event in our data that occurred in this specific scenario and produced this outcome. For any given scenario (T, ΔT) there is a 100% probability that exactly one of the discretized outcomes will occur, so we divide the number of times we observe a given outcome by the total number of outcomes we observed over all our data for that scenario. Applying this analysis to all of the > 26,000 movements in our radial gradient dataset yielded a densely sampled matrix of posterior probabilities for dwell time, displacement, turn magnitude, and turn direction bias under every possible thermosensory scenario. To improve the posterior probability matrix for rare thermosensory scenarios or rare outcome values (e.g. a dwell time of 9.8 s), we applied moderate smoothing with a sliding box filter across T, ΔT, and locomotor element value. To progressively build up to the complete model with all possible thermosensory relationships, we also generated a simpler distribution for each motor element in which we counted the number of times we observed a movement where the motor element had a particular value and then divided by the number of movements in our radial gradient dataset. This simpler distribution does not take into account any modulation of the locomotor element by thermosensory experience, but it is still realistic in the sense that our Monte Carlo simulations will select a certain value for a given motor element with the same frequency with which we observe that value overall in our dataset.

5. Discussion and future directions

1 ABSTRACT

Our results show that larval zebrafish can effectively navigate a thermal gradient using only thermosensory cues. We dissected the components of larval locomotion and found that absolute and relative thermosensory information modulates every locomotor element that we considered, but in distinct ways. Taken together, these sensorimotor relationships represent a coherent strategy for thermal navigation. Our behavioral description of thermosensory modulation of dwell time, displacement, turn magnitude, and turn direction bias suggests the existence of distinct locomotor subsystems in the zebrafish brain with specific interactions with the thermosensory circuitry. We propose to elucidate the circuits underlying these locomotor subsystems and sensorimotor relationships using a combination of functional imaging and circuit tracing.

2 MAJOR CONCLUSIONS

We have established an assay for thermal navigation in larval zebrafish. We have shown that zebrafish can navigate away from noxious heat and toward the preferred temperature zone while relying exclusively on thermosensory information in the absence of visual or other cues. We identified four locomotor elements that are modulated by either absolute or relative thermal experience and demonstrated that these sensorimotor relationships persist in an open loop setting. This work establishes a system for studying thermosensory behavior in larval zebrafish as well as navigation behaviors in general. We can also begin to ask what underlying neural circuitry mediates the specific sensorimotor relationships we observe. In this chapter, we will discuss experimental strategies for studying the neural circuitry of thermal navigation with functional imaging. This will require the

development of a thermosensory assay that can be applied to tethered animals while imaging is being performed.

3 FURTHER BEHAVIORAL CHARACTERIZATION

Can our model predict navigation performance in novel assays?

Our data suggest that modulation of turn magnitude and turn direction bias by T and ΔT underlies thermal navigation in zebrafish larvae. This modulation was observed both in the radial gradient as well as in response to purely temporal changes in temperature in the uniform thermal waveform chamber. This suggests that the behavioral rules we have uncovered are driven directly by thermal stimuli and represent an innate thermotactic strategy. To further test this hypothesis, one can determine whether the same strategy is used in different spatial gradients. To this end, we have begun to design thermal gradient chambers with different spatial layouts. For example, to test the hypothesis that turn magnitude and turn direction bias are general solutions to thermal navigation, we will construct a linear gradient assay flanked on both sides by noxious heat (**Fig. 33**). The ideal trajectories in this linear gradient are parallel lines along the midline of the chamber (**Fig. 31a**). However, the navigational trajectories predicted by our model are strikingly different. Our model, based on turn magnitude and turn direction bias, predicts that zebrafish would navigate this environment by circling the midline according to the preferred turn direction (**Fig. 31b**). The results of these experiments will strengthen our model of thermal navigation. If turn rate and turn direction bias have the same role in the linear gradient assay as they do in the radial gradient assay, we will have independent confirmation of the sensorimotor relationships we inferred previously. If locomotor elements such as turn magnitude and turn direction bias are not evident or apply differently in the linear gradient assay, we will refine our model to reflect which relationships are fixed across navigation tasks and which relationships are task specific.

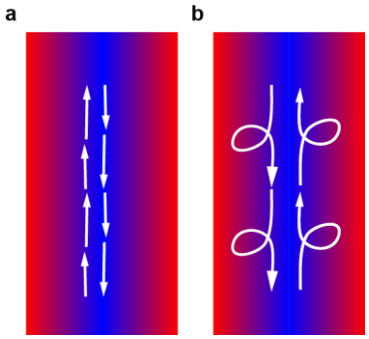

Figure 33 | Hypothetical navigational trajectories in a linear thermal gradient. a, Ideal trajectories run parallel to 25 °C isotherm along the chamber midline. **b,** Predicted navigational trajectories if fish modulate turn magnitude and turn direction bias in response to thermosensory experience.

What is the behavioral strategy underlying positive thermotaxis?

In *C. elegans*, positive thermotaxis is only expressed under specific sets of conditions, while in Drosophila larvae, positive thermotaxis appears to be as robust as negative thermotaxis. Based on our previous data from thermal gradients between 15 °C and 37 °C, larval zebrafish are capable of positive thermotaxis. We have yet to determine the robustness of positive thermotaxis across animals and the underlying behavioral strategy. The behavioral strategy used during negative thermotaxis raises some interesting questions for positive thermotaxis. Is the preferred turn direction during rising temperatures in negative thermotaxis also the preferred turn direction during rising temperatures in positive thermotaxis? The answer to this question would determine whether the preferred turn direction we observe is a response to noxious temperatures regardless of the sign of temperature change or a response to strictly rising temperatures. If larval zebrafish maintain a preferred turn direction in response to strictly rising temperatures, we would expect the same turn direction bias in response to rising temperatures in both positive and negative thermotaxis. If larval zebrafish maintain a preferred turn direction in response to noxious changes in temperature or unfavorable headings, then we would expect the preferred turn direction during rising temperatures in negative thermotaxis to be the same

as the preferred turn direction during falling temperatures in positive thermotaxis. For this experiment to work, we may need to examine subsets of animals with fairly stable turn direction preferences.

Is the thermotaxis strategy common to other forms of navigation?

There is extensive overlap in the circuitry and molecular machinery that underlie chemotaxis and thermotaxis in both *E.coli*[1-2,88] and *C.elegans*[8,34,38-40,]. In many cases, it would appear that the same navigation strategies are appropriated by two different sensory stimuli. For example, in *E. coli*, the biased random walk strategy is observed in both thermotaxis and chemotaxis. In fact, the methyl-accepting chemotaxis protein (MCP) acts as a thermosensor in thermatoxis[1-2]. MCP interacts with downstream proteins CheA and CheP to control the direction of flagella rotation in both chemotaxis and thermotaxis. In *C. elegans*, biased random walking and weathervaning are observed in both thermotaxis and chemotaxis[7,19,39]. AFD and AWC neurons report both thermosensory and chemosensory stimuli, and downstream neurons such as AIY are involved in both behaviors[7,34,38-40,]. In both of these systems, it appears that a general set of locomotor strategies is present, and can be activated by different modalities of sensory stimuli. A possible explanation for this overlap in behavioral strategies is that these organisms have a limited number of neurons or molecular components to implement multiple distinct strategies for each form of navigation. Determining whether a similar phenomenon is observed in more complex animals with several orders of magnitude more neurons may provide some interesting insights into this question.

In larval zebrafish, no quantitative study of chemotaxis has been performed. Therefore, it remains to be seen whether the strategy we observe in thermotaxis is also employed in navigation using other sensory modalities. Based on the other model systems, it's highly likely that at least some elements of the behavioral strategies will be shared across different modalities. The answer to this question could hint at the neural circuitry that underlies navigation. Is there a core circuit for modulating

turn magnitude and turn direction bias, which can be accessed by different sensory modalities? Alternatively, is each modality performing a unique sensorimotor transformation mediated by independent circuit elements?

What is the stability of turn direction bias?

Our results indicate that bias toward a preferred turn direction during rising temperatures is stable over a time scale of minutes. Transitions from preferring one direction to another can be observed in the thermal gradient, and different animals exhibit different levels of stability. About one third of animals exhibit a stable preference for approximately 30 min, while the majority of animals exhibit 1-2 switches in direction preference (**Fig. 26**). Increased sample size in both the radial gradient and sine wave protocol will allow us to determine the average stability of a given turn direction preference, and the variability across the population. Longer protocols may allow us more accurately determine the stability of turn direction preference for each individual animal.

What is the thermal sensitivity of larval zebrafish?

Both *C. elegans* and *Drosophila* larvae are sensitive to very small changes in temperature (<0.005°C/sec)[7]. Our current assays do not attempt to determine the resolution of zebrafish thermal sensitivity. However, we can easily extend our analysis to determine the limit of zebrafish thermal sensitivity. For example, we can determine whether zebrafish larvae can navigate to their preferred temperature in a gradient with a much shallower slope. The average displacement of zebrafish in a single movement in the radial gradient is 4 mm. In our current thermal gradient, this corresponds to a temperature change per bout of -0.64 °C to +0.64 °C depending on the orientation of the animal. We can determine whether zebrafish can navigate to their preferred temperature in gradients where the maximum temperature change per bout is much lower (e.g. 0.1°C). A more systematic way of testing for the sensitivity of larval zebrafish is to simply correlate locomotor elements such as turn magnitude with

temporal changes in temperature. For example, we can deliver sine waves with decreasing amplitudes, and determine the amplitude at which turn magnitude becomes indistinguishable between the rising and falling phase of the sine wave. This point would represent the thermal sensitivity limit of larval zebrafish.

4 PROSPECTS FOR CALCIUM IMAGING

Our quantitative analysis of zebrafish thermal navigation behavior predicts the existence of specific circuit elements related to thermosensory processing and locomotor decision making. Since the functional organization of the larval zebrafish brain is not yet well understood, the most promising way to identify neurons belonging to these circuits is by comprehensive whole brain calcium imaging. Recent progress in genetically encoded calcium indicators have increased sensitivity and brightness to a point where even weak neural activity and single action potentials can be detected[89-94]. We are pioneers of whole brain imaging in larval zebrafish, having established a cloning system to place the ever-improving GCaMP variants under the control of a large pan-neuronal promoter, flanked by transposon recognition arms for efficient transgenesis[87]. We have established transgenics for GCaMP2, GCaMP3, and GCaMP5 and expect that soon we will recover our first GCaMP6 transgenics.

The remaining challenge before we can begin collecting functional data is that we must adapt the free swimming behavioral assay so that zebrafish can still perform the behavior while tethered under a stationary microscope. We have recently developed the ability to collect functional data from tethered animals while allowing them to freely move their tail. We mitigate the effects of stimulus-induced and motor-induced motion artifacts using online focal plane adjustment and offline lateral adjustment. Our imaging system allows us to stably monitor an arbitrary field of neurons in the brain for hours while animals generate tail free behavior.

There are two strategies that would allow us to gain insights into thermal navigation by calcium imaging. A complicated approach is to use a closed loop virtual reality system to track the tail of a tethered fish in parallel with calcium imaging, so that decoded tail movements can be used to update the position and heading of the animal in a virtual thermal gradient and update the temperature of the animal according to its position in the virtual gradient. We have already developed a working implementation of this closed loop setup and performed pilot experiments which suggest that tethered animals can show thermal restriction, although further work is needed to determine how well it works across a larger number of animals.

An alternative approach that would be much simpler is to simply present thermal steps and sine waves in open loop while recording neural activity and locomotor output. Our behavioral results in the open loop thermal waveform chamber would argue that the mechanisms at work during thermal navigation are also activated by open loop thermal stimulation. We will continue to explore both the closed and open loop approaches to studying thermal navigation in tethered animals.

5 EXPECTED OUTCOMES OF CALCIUM IMAGING

On the sensory side, our dissection of the thermal stimulus suggests that there should be neural representation of both absolute and relative temperature. Our imaging efforts to date suggest that the primary sensory neurons of the trigeminal ganglion that respond to thermal stimulation respond to absolute but not relative temperature, suggesting that the ability to modulate locomotion based on relative changes in temperature arises downstream of the primary sensory neurons. Based on preliminary studies, we expect that in response to open loop sine wave thermal stimulation, some neurons in the hindbrain and forebrain will show activation that is most correlated to relative temperature changes, rather than absolute temperature. In contrast, we expect that the majority of

neurons in the dorsal hindbrain that show activity related to temperature will be most correlated to absolute temperature.

On the locomotor side, the most interesting strategy is the turn direction bias. We would like to comprehensively image the brain to search for activity signals that correlate with the preferred turn direction. Here we can exploit the stability of our imaging setup to monitor the activity of each neuron long enough to observe one or more spontaneous switches in turn direction. We will also monitor the tail output throughout the imaging experiment so that we can analyze the preferred turn direction and identify the times during the experiment when the turn direction switches. We will look for neurons that show prolonged activation during one preferred turn direction and are less active when the turn direction switches. Alternatively, we may find neurons that show a transient change in activity specifically at the time of the transition in preferred turn direction. These neurons may promote switching the preferred turn direction from one direction to the other.

REFERENCES

1. Mizuno T, Imae Y. Conditional inversion of the thermoresponse in Escherichia coli. 1984 Jul;159(1):360-7.

2. Maeda K, Imae Y. Thermosensory transduction in Escherichia coli: inhibition of the thermoresponse by L-serine. Proc Natl Acad Sci U S A. 1979 Jan;76(1):91-5.

3. Berg HC, Brown DA: Chemotaxis in E. coli analysed by threedimensional tracking. Nature 1972, 239:500-504.

4. Signal transduction in bacterial chemotaxis. Baker MD, Wolanin PM, Stock JB.

5. Wadhams GH, Armitage JP. Making sense of it all: Bacterial chemotaxis. Nat Rev Mol Cell Biol 2004 5:1024-1037.

6. Salman H, Libchaber A. A concentration-dependent switch in the bacterial response to temperature. Nat Cell Biol. 2007 Sep;9(9):1098-100.

7. Garrity PA, Goodman MB, Samuel AD, Sengupta P. Running hot and cold: behavioral strategies, neural circuits, and the molecular machinery for thermotaxis in C. elegans and Drosophila. Genes & Dev. 2010;24(21):2365-82.

8. Hedgecock EM, Russell RL. Normal and Mutant Thermotaxis in the Nematode Caenorhabditis elegans. Proc Natl Acad Sci. 1975;72(1):4061-5--5.

9. Ryu WS, Samuel AD. Thermotaxis in Caenorhabditis elegans analyzed by measuring responses to defined Thermal stimuli. J Neurosci. 2002;22(13):5727-33.

10. Ramot D, MacInnis BL, Lee HC, Goodman MB. Thermotaxis is a robust mechanism for thermoregulation in Caenorhabditis elegans nematodes. J Neurosci. 2008;28(47):12546-57.

11. Yamada Y, Ohshima Y. Distribution and movement of Caenorhabditis elegans on a thermal gradient. J Exp Biol. 2003 Aug; 206(Pt 15):2581-93.

12. Stephens GJ, Johnson-Kerner B, Bialek W, Ryu WS. Dimensionality and dynamics in the behavior of C. elegans. PLoS Comput Biol. 2008 Apr 25; 4(4):e1000028.

13. Ghosh R, Mohammadi A, Kruglyak L, Ryu WS. Multiparameter behavioral profiling reveals distinct thermal response regimes in Caenorhabditis elegans. BMC Biol. 2012 Oct 31;10:85.

14. McCormick KE, Gaertner BE, Sottile M, Phillips PC, Lockery SR. Microfluidic devices for analysis of spatial orientation behaviors in semi-restrained Caenorhabditis elegans. PLoS One. 2011;6(10):e25710.

15. Zariwala HA, Miller AC, Faumont S, Lockery SR. Step response analysis of thermotaxis in Caenorhabditis elegans. J Neurosci. 2003 May 15;23(10):4369-77.

16. Jurado P, Kodama E, Tanizawa Y, Mori I. Distinct thermal migration behaviors in response to different thermal gradients in Caenorhabditis elegans. Genes Brain Behav. 2010 Feb;9(1):120-7.

17. Nakazato K, Mochizuki A. Steepness of thermal gradient is essential to obtain a unified view of thermotaxis in C. elegans. J Theor Biol. 2009 Sep 7;260(1):56-65.

18. Anderson JL, Albergotti L, Proulx S, Peden C, Huey RB, Phillips PC. Thermal preference of Caenorhabditis elegans: a null model and empirical tests. J Exp Biol. 2007 Sep; 210(Pt 17):3107-16

19. Luo L, Clark DA, Biron D, Mahadevan L, Samuel AD. Sensorimotor control during isothermal tracking in Caenorhabditis elegans. J Exp Biol. 2006;209(Journal Article):4652-62.

20. Mori I, Ohshima Y. Neural regulation of thermotaxis in Caenorhabditis elegans. Nature (London). 1995;376(6538):344-8.

21. Coburn CM, Bargmann CI. A putative cyclic nucleotide-gated channel is required for sensory development and function in C. elegans. Neuron. 1996 Oct; 17(4):695-706.

22. Komatsu H, Mori I, Rhee JS, Akaike N, Ohshima Y. Mutations in a cyclic nucleotide-gated channel lead to abnormal thermosensation and chemosensation in C. elegans. Neuron. 1996 Oct; 17(4):707-18.

23. Kimura KD, Miyawaki A, Matsumoto K, Mori I. The C. elegans thermosensory neuron AFD responds to warming. Curr Biol. 2004 Jul 27;14(14):1291-5.

24. Clark DA, Biron D, Sengupta P, Samuel AD. The AFD sensory neurons encode multiple functions underlying thermotactic behavior in Caenorhabditis elegans. J Neurosci. 2006;26(28):7444-51.

25. Samuel AD, Sengupta P. Sensorimotor integration: locating locomotion in neural circuits. curr biol. 2005;15(9):R341-3.

26. Biron D, Shibuya M, Gabel C, Wasserman SM, Clark DA, Brown A, Sengupta P, Samuel AD. A diacylglycerol kinase modulates long-term thermotactic behavioral plasticity in C. elegans. Nat Neurosci. 2006 Dec; 9(12):1499-505.

27. Chung SH, Clark DA, Gabel CV, Mazur E, Samuel AD. The role of the AFD neuron in C. elegans thermotaxis analyzed using femtosecond laser ablation. BMC Neurosci. 2006;7(1):30-.

28. Clark DA, Gabel CV, Gabel H, Samuel AD. Temporal activity patterns in thermosensory neurons of freely moving Caenorhabditis elegans encode spatial thermal gradients. J Neurosci. 2007;27(23):6083-90.

29. Chalasani SH, Chronis N, Tsunozaki M, Gray JM, Ramot D, Goodman MB, Bargmann CI. Dissecting a circuit for olfactory behaviour in Caenorhabditis elegans. Nature. 2007 Nov 1; 450(7166):63-70.

30. Kuhara A, Okumura M, Kimata T, Tanizawa Y, Takano R, Kimura KD, Inada H, Matsumoto K, Mori I. Temperature sensing by an olfactory neuron in a circuit controlling behavior of C. elegans. Science. 2008 May 9; 320(5877):803-7.

31. Ramot D, MacInnis BL, Goodman MB 2008a. Bidirectional temperature-sensing by a single thermosensory neuron in C. elegans. Nat Neurosci 11: 908-915.

32. Clark DA, Gabel CV, Lee TM, Samuel AD. Short-term adaptation and temporal processing in the cryophilic response of Caenorhabditis elegans. J Neurophysiol. 2007;97(3):1903-10.

33. Ito H, Inada H, Mori I. Quantitative analysis of thermotaxis in the nematode Caenorhabditis elegans. J Neurosci Methods. 2006 Jun 30;154(1-2):45-52.

34. Mori I. Genetics of chemotaxis and thermotaxis in the nematode Caenorhabditis elegans. Annu Rev Genet. 1999;33:399-422.

35. Stegeman GW, Bueno de Mesquita M, Ryu WS, Cutter AD. Temperature-dependent behaviours are genetically variable in the nematode Caenorhabditis briggsae. J Exp Biol. 2012 Nov 15.

36. Mohri A, Kodama E, Kimura KD, Koike M, Mizuno T, Mori I. Genetic control of temperature preference in the nematode Caenorhabditis elegans. Genetics. 2005 Mar;169(3):1437-50.

37. Schneider MJ, Fontana DR, Poff KL. Mutants of thermotaxis in Dictyostelium discoideum. Exp Cell Res. 1982 Aug;140(2):411-6.

38. Gray JM, Hill JJ, Bargmann CI. A circuit for navigation in Caenorhabditis elegans. Proc Natl Acad Sci U S A. 2005;102(9):3184-91. PMCID: 546636.

39. Iino Y, Yoshida K. Parallel use of two behavioral mechanisms for chemotaxis in Caenorhabditis elegans. J Neurosci. 2009 Apr 29;29(17):5370-80.

40. Adachi R, Osada H, Shingai R. Phase-dependent preference of thermosensation and chemosensation during simultaneous presentation assay in Caenorhabditis elegans. BMC Neurosci. 2008 Nov 1;9:106.

41. Ohnishi N, Kuhara A, Nakamura F, Okochi Y, Mori I. Bidirectional regulation of thermotaxis by glutamate transmissions in Caenorhabditis elegans. EMBO J. 2011 Apr 6;30(7):1376-88.

42. Nishida Y, Sugi T, Nonomura M, Mori I. Identification of the AFD neuron as the site of action of the CREB protein in Caenorhabditis elegans thermotaxis. EMBO Rep. 2011 Jul 8;12(8):855-62.

43. Cassata G, Kagoshima H, Andachi Y, Kohara Y, Dürrenberger MB, Hall DH, Bürglin TR. The LIM homeobox gene ceh-14 confers thermosensory function to the AFD neurons in Caenorhabditis elegans. Neuron. 2000 Mar;25(3):587-97.

44. Liu S, Schulze E, Baumeister R. Temperature- and touch-sensitive neurons couple CNG and TRPV channel activities to control heat avoidance in Caenorhabditis elegans. PLoS One. 2012;7(3):e32360.

45. White JG, Southgate E, Thomson JN, Brenner S. 1986. The structure of the nervous system of the nematode Caenorhabditis elegans. Philos Trans R Soc Lond B 314: 1-340.

46. Yoshifumi Okochi, Koutarou D Kimura, Akane Ohta, and Ikue Mori. Diverse regulation of sensory signaling by C. elegans nPKC-epsilon/eta TTX-4. EMBO J. 2005 June 15; 24(12): 2127-2137.

47. Satterlee, J.S. et al. Specification of thermosensory neuron fate in C. elegans requires ttx-1, a homolog of otd/Otx. Neuron 31, 943-956 (2001).

48. Hobert O, Mori I, Yamashita Y, Honda H, Ohshima Y, Liu Y, Ruvkun G. Regulation of interneuron function in the C. elegans thermoregulatory pathway by the ttx-3 LIM homeobox gene. Neuron. 1997 Aug;19(2):345-57.

49. Biron D, Wasserman S, Thomas JH, Samuel AD, Sengupta P. An olfactory neuron responds stochastically to temperature and modulates Caenorhabditis elegans thermotactic behavior. Proc Natl Acad Sci U S A. 2008 Aug 5;105(31):11002-7

50. Mehta SB, Whitmer D, Figueroa R, Williams BA, Kleinfeld D (2007) Active spatial perception in the vibrissa scanning sensorimotor system. PLoS Biol 5:15.

51. Nagel G, Brauner M, Liewald JF, Adeishvili N, Bamberg E, Gottschalk A (2005) Light activation of channelrhodopsin-2 in excitable cells of Caenorhabditis elegans triggers rapid behavioral responses. Curr Biol 15: 2279-2284.

52. Leifer AM, Fang-Yen C, Gershow M, Alkema MJ, Samuel AD. Optogenetic manipulation of neural activity in freely moving Caenorhabditis elegans. Nat Methods. 2011 Feb;8(2):147-52

53. Kocabas A, Shen CH, Guo ZV, Ramanathan S. Controlling interneuron activity in Caenorhabditis elegans to evoke chemotactic behaviour. Nature. 2012 Oct 11;490(7419):273-7

54. Donnelly JL, Clark CM, Leifer AM, Pirri JK, Haburcak M, Francis MM, Samuel AD, Alkema MJ. Monoaminergic Orchestration of Motor Programs in a Complex C. elegans Behavior. PLoS Biol. 2013 Apr;11(4):e1001529

55. Zhang F, Wang LP, Brauner M, Liewald JF, Kay K, Watzke N, Wood PG, Bamberg E, Nagel G, Gottschalk A, Deisseroth K (2007) Multimodal fast optical interrogation of neural circuitry. Nature 446: 633-639.

56. Luo L, Gershow M, Rosenzweig M, Kang K, Fang-Yen C, Garrity PA, et al. Navigational decision making in Drosophila thermotaxis. J Neurosci. 2010;30(12):4261-72.

57. Lahiri S, Shen K, Klein M, Tang A, Kane E, Gershow M, Garrity P, Samuel AD. Two alternating motor programs drive navigation in Drosophila larva. PLoS One. 2011;6(8):e23180.

58. Liu L, Yermolaieva O, Johnson WA, Abboud FM, Welsh MJ 2003. Identification and function of thermosensory neurons in Drosophila larvae. Nat Neurosci 6: 267-273

59. Liu L, Yermolaieva O, Johnson WA, Abboud FM, Welsh MJ. Identification and function of thermosensory neurons in Drosophila larvae. Nat Neurosci. 2003 Mar; 6(3):267-73.

60. Kwon Y, Shen WL, Shim HS, Montell C. Fine thermotactic discrimination between the optimal and slightly cooler temperatures via a TRPV channel in chordotonal neurons. J Neurosci. 2010 Aug 4; 30(31):10465-71.

61. Rosenzweig M, Brennan KM, Tayler TD, Phelps PO, Patapoutian A, Garrity PA. The Drosophila ortholog of vertebrate TRPA1 regulates thermotaxis. Genes Dev. 2005 Feb 15;19(4):419-24.

62. Terrien J, Perret M, Aujard F. Behavioral thermoregulation in mammals: a review. Front Biosci. 2011 Jan 1;16:1428-44.

63. Moqrich A, Hwang SW, Earley TJ, Petrus MJ, Murray AN, Spencer KS, Andahazy M, Story GM, Patapoutian A. Impaired thermosensation in mice lacking TRPV3, a heat and camphor sensor in the skin. Science. 2005 Mar 4;307(5714):1468-72.

64. Lee H, Iida T, Mizuno A, Suzuki M, Caterina MJ. Altered thermal selection behavior in mice lacking transient receptor potential vanilloid 4. J Neurosci. 2005 Feb 2;25(5):1304-10.

65. Johanson IB. Thermotaxis in neonatal rat pups. Physiol Behav. 1979 Nov;23(5):871-4.

66. Leonard CM. Thermotaxis in golden hamster pups. J Comp Physiol Psychol. 1974 Mar;86(3):458-69.

67. Gumma MR, South FE, Allen JN. Temperature preference in golden hamsters. Anim Behav. 1967 Oct;15(4):534-7.

68. R. Refinetti: Body temperature and behavior of golden-hamsters (Mesocricetus-auratus) and ground-squirrels (Spermophilus-tridecemlineatus) in a thermal gradient. Journal of Comparative Physiology a-Sensory Neural and Behavioral Physiology, 177(6), 701-705 (1995)

69. Ward AJ, Hensor EM, Webster MM, Hart PJ. Behavioural thermoregulation in two freshwater fish species. J Fish Biol. 2010 Jun;76(10):2287-98.

70. Prober DA, Zimmerman S, Myers BR, McDermott BM, Jr., Kim SH, Caron S, et al. Zebrafish TRPA1 channels are required for chemosensation but not for thermosensation or mechanosensory hair cell function. J Neurosci. 2008;28(40):10102-10. PMCID: 2728686.

71. Fetcho JR, Higashijima S, McLean DL. Zebrafish and motor control over the last decade. Brain Res Rev. 2008 Jan;57(1):86-93.

72. Liu YC, Bailey I, Hale ME. Alternative startle motor patterns and behaviors in the larval zebrafish (Danio rerio). J Comp Physiol A Neuroethol Sens Neural Behav Physiol. 2012 Jan;198(1):11-24.

73. Budick SA, O'Malley DM. Locomotor repertoire of the larval zebrafish: swimming, turning and prey capture. J Exp Biol. 2000 Sep;203(Pt 17):2565-79.

74. Dhaka A, Viswanath V, Patapoutian A. Trp ion channels and temperature sensation. Annu Rev Neurosci. 2006;29:135-61.

75. Lumpkin EA, Caterina MJ. Matsuura H, Sokabe T, Kohno K, Tominaga M, Kadowaki T. Mechanisms of sensory transduction in the skin. Nature. 2007 Feb 22;445(7130):858-65.

76. Bandell M, Macpherson LJ, Patapoutian A. From chills to chilis: mechanisms for thermosensation and chemesthesis via thermoTRPs. Curr Opin Neurobiol. 2007 Aug;17(4):490-7.

77. Saito S, Shingai R. Evolution of thermoTRP ion channel homologs in vertebrates. Physiol Genomics. 2006 Nov 27;27(3):219-30.

78. Andermann et al., 2002 Andermann, P., Ungos, J., and Raible, D.W. (2002). Neurogenin1 defines zebrafish cranial sensory ganglia precursors. Dev. Biol. 251, 45-58.

79. Knaut H, Blader P, Strähle U, Schier AF. Assembly of trigeminal sensory ganglia by chemokine signaling. Neuron. 2005 Sep 1;47(5):653-66.

80. Weis JS. Analysis of the development of nervous system of the zebrafish, Brachydanio rerio. I. The normal morphology and development of the spinal cord and ganglia of the zebrafish. J Embryol Exp Morphol. 1968 Apr;19(2):109-19.

81. An M, Luo R, Henion PD. Differentiation and maturation of zebrafish dorsal root and sympathetic ganglion neurons. J Comp Neurol. 2002 May 6;446(3):267-75.

82. Bernhardt RR, Chitnis AB, Lindamer L, Kuwada JY. Identification of spinal neurons in the embryonic and larval zebrafish. J Comp Neurol. 1990 Dec 15;302(3):603-16.

83. J. Lamborghini. Disappearance of Rohon Beard neurons from the spinal cord of larval Xenopus laevis. J. Comp. Neurol., 246 (1987), pp. 47-55

84. Gau P, Poon J, Ufret-Vincenty C, Snelson CD, Gordon SE, Raible DW, Dhaka A. The zebrafish ortholog of TRPV1 is required for heat-induced locomotion. J Neurosci. 2013 Mar 20;33(12):5249-60

85. Baier H, Scott EK. Genetic and optical targeting of neural circuits and behavior--zebrafish in the spotlight. Curr Opin Neurobiol. 2009;19(5):553-60. PMCID: 2787859.

86. Schoonheim PJ, Arrenberg AB, Del Bene F, Baier H. Optogenetic localization and genetic perturbation of saccade-generating neurons in zebrafish. J Neurosci. 2010;30(20):7111-20.

87. Ahrens MB, Li JM, Orger MB, Robson DN, Schier AF, Engert F, Portugues R. Brain-wide neuronal dynamics during motor adaptation in zebrafish. Nature. 2012 May 9;485(7399):471-7.

88. Sourjik V, Wingreen NS. Responding to chemical gradients: bacterial chemotaxis. Curr Opin Cell Biol. 2012 Apr;24(2):262-8.

89. Burgess HA, Schoch H, Granato M. Distinct retinal pathways drive spatial orientation behaviors in zebrafish navigation. Curr Biol. 2010 Feb 23;20(4):381-6.

90. Tian L, Hires SA, Mao T, Huber D, Chiappe ME, Chalasani SH, et al. Imaging neural activity in worms, flies and mice with improved GCaMP calcium indicators. Nat Methods. 2009;6(12):875-81.

91. Miyawaki A, Llopis J, Heim R, McCaffery JM, Adams JA, Ikura M, Tsien RY. Fluorescent indicators for Ca2+ based on green fluorescent proteins and calmodulin. Nature. 1997 Aug 28;388(6645):882-7.

92. Mank M, Santos AF, Direnberger S, Mrsic-Flogel TD, Hofer SB, Stein V, Hendel T, Reiff DF, Levelt C, Borst A, Bonhoeffer T, Hübener M, Griesbeck O. A genetically encoded calcium indicator for chronic in vivo two-photon imaging. Nat Methods. 2008 Sep;5(9):805-11.

93. Nagai T, Sawano A, Park ES, Miyawaki A. Circularly permuted green fluorescent proteins engineered to sense Ca2+. Proc Natl Acad Sci U S A. 2001 Mar 13;98(6):3197-202.

94. Akerboom J, Chen TW, Wardill TJ, Tian L, Marvin JS, Mutlu S, Calderón NC, Esposti F, Borghuis BG, Sun XR, Gordus A, Orger MB, Portugues R, Engert F, Macklin JJ, Filosa A, Aggarwal A, Kerr RA, Takagi R, Kracun S, Shigetomi E, Khakh BS, Baier H, Lagnado L, Wang SS, Bargmann CI, Kimmel BE, Jayaraman V, Svoboda K, Kim DS, Schreiter ER, Looger LL. Optimization of a GCaMP Calcium Indicator for Neural Activity Imaging. J Neurosci. 2012 Oct 3;32(40):13819-13840..